END
DATE
FILMED
2-81
DTIC

REPORT DOCUMENTATION PAGE		READ INSTRUCTIONS BEFORE COMPLETING FORM
1. REPORT NUMBER AFGL-TR-79-0286	2. GOVT ACCESSION NO. AD-A082 913	3. RECIPIENT'S CATALOG NUMBER
4. TITLE (and Subtitle) GEOPHYSICAL FIBER INTERFEROMETER GYROSCOPE.		5. TYPE OF REPORT & PERIOD COVERED 9/27/78 - 9/30/79 FINAL
		6. PERFORMING ORG. REPORT NUMBER GSL-79-013
7. AUTHOR(s) LAWRENCE D. WEAVER		8. CONTRACT OR GRANT NUMBER(s) F 19628-78-C-0236
9. PERFORMING ORGANIZATION NAME AND ADDRESS Geospace Sciences Laboratory University of Utah Research Institute 420 Chipeta Way, Suite 160, SLC, UT 84108		10. PROGRAM ELEMENT, PROJECT, TASK AREA & WORK UNIT NUMBERS 62101F 760006AS
11. CONTROLLING OFFICE NAME AND ADDRESS Air Force Geophysics Laboratory Hanscom AFB, Massachusetts 1731 Monitor/Dr. James A. Hammond/LWG		12. REPORT DATE December 31, 1979
		13. NUMBER OF PAGES 79
14. MONITORING AGENCY NAME & ADDRESS(if different from Controlling Office)		15. SECURITY CLASS. (of this report) UNCLASSIFIED
		15a. DECLASSIFICATION/DOWNGRADING SCHEDULE

16. DISTRIBUTION STATEMENT (of this Report)

Approved for public release; distribution unlimited.

17. DISTRIBUTION STATEMENT (of the abstract entered in Block 20, if different from Report)

18. SUPPLEMENTARY NOTES

19. KEY WORDS (Continue on reverse side if necessary and identify by block number)

Rotation sensor, gyroscope, fiber gyroscope, laser interferometer gyroscope, North-seeker, single mode fibers, Sagnac effect.

20. ABSTRACT (Continue on reverse side if necessary and identify by block number)

This report describes a development effort of the University of Utah Research Institute aimed at perfecting a North-seeking device based on the passive interferometer gyroscope concept. The rotation sensing mechanism of the interferometer is based on the Sagnac effect.

The form of the interferometer is a fiber ring. The performance requirements of the device are developed in terms of the desired pointing accuracy vs.

measurement resolution or sensitivity. The interferometer performance will be compared to that of a typical ring-laser gyro.

Methods by which the sensitivity of the interferometer could be potentially increased will be discussed. Two of these methods, namely the electro-optic phase shifter and acousto-optic frequency shifter, were evaluated and their limitations regarding the performance of a fiber interferometer gyroscope will be addressed. Additionally, signal processing requirements will also be discussed.

Finally, the theoretical limit for performance of a fiber-optic interferometer will be discussed in terms of the so-called "photon noise limit." This is the limit to performance that several researchers have alluded to in arriving at the ultimate sensitivity of a passive interferometer laser gyroscope. Suggestions for a device in which the photon noise limit may be approached will also be discussed.

Accession For	
NTIS GRA&I	X
DDC TAB	☐
Unannounced	☐
Justification	
By	
Distribution/	
Availability Codes	
Dist.	Avail and/or special
A	

TABLE OF CONTENTS

LIST OF FIGURES

1.0 INTRODUCTION

This report describes a development effort at the Geospace Sciences Laboratory of the University of Utah Research Institute aimed at perfecting a North-seeking device based on the passive interferometer gyroscope concept. The rotation sensing mechanism of the interferometer is based on the Sagnac effect.[1]

The form of the interferometer is a fiber ring. The performance requirements of the device are developed in terms of the desired pointing accuracy vs. measurement resolution or sensitivity. The interferometer performance will be compared to that of a typical ring-laser gyro.

Methods by which the sensitivity of the interferometer could be potentially increased will be discussed. Two of these methods, namely the electro-optic phase shifter and acousto-optic frequency shifter, were evaluated and their limitations re the performance of a fiber interferometer gyroscope will be addressed. Additionally, signal processing requirements will also be discussed.

Finally, the theoretical limit for performance of a fiber-optic interferometer will be discussed in terms of the so-called "photon noise limit". This is the limit to performance that several researchers have alluded to in arriving at the ultimate sensitivity of a passive interferometer laser gyroscope. Suggestions for a device in which the photon noise limit may be approached will also be discussed.

2.0 OPTICAL ROTATION SENSORS

To date, the overwhelming majority of rotation sensing devices (gyroscopes) have been of the rotating mass type. However, with the advent of lasers and single mode optical waveguides (fibers), optical rotation sensors have become

1

feasible and potentially very attractive for some applications. Indeed, ring-laser gyros have passed into the application phase. In the following sections, two types of rotation sensors will be discussed: the ring-laser gyro, and the ring interferometer gyro. Both types depend on the Sagnac effect for their operation.

2.1 Sagnac Effect

In 1913, Sagnac[1] demonstrated that a ring interferometer (See Figure 1)
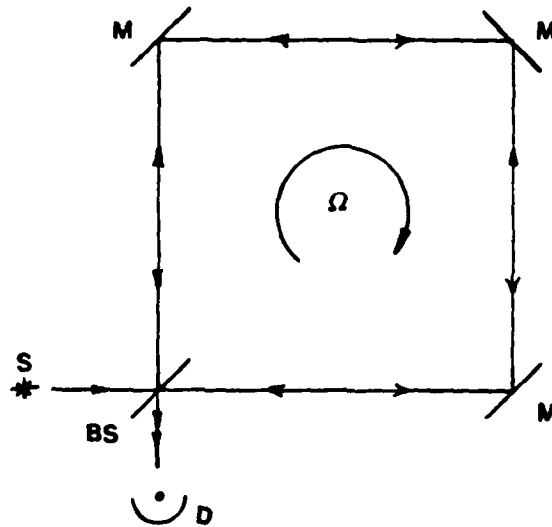
Figure 1. Sagnac interferometer schematic. This is the original form of interferometer used to study the Sagnac effect.

in rotation about any axis normal to the interferometer gives rise to a fringe shift as compared to the case when the interferometer is stationary. Analyses based on classical theory, special relativity or general relativity, all agree to first order. They show that rotation of the interferometer gives rise to a transit time difference for light traversing the ring in the CW and CCW

2

directions of

$$\Delta t = \frac{4A\Omega}{c^2} \; . \qquad\qquad (1)$$

In Equation (1), A is the area enclosed by the ring, Ω is the rotation rate, and c is the speed of light. The salient features of the effect are:

a) Equation (1) is correct.

b) The result is independent of the shape of the area, A.

c) The result does not depend on the location of the axis of rotation.

d) The result does not depend on the presence of a co-moving refracting medium in the beam path.

Many physicists[2] have contributed to the analyses and experiments that have verified the features listed above. Post[3], in a 1967 Review of Modern Physics article, presented a complete discussion of the Sagnac effect including various subcases (e.g., moving ring interferometer with co-moving medium, etc.). The Sagnac effect is well established and understood.

2.2 Ring-Laser Rotation Sensor

Consider a suitably-shaped ring (e.g., an equilateral triangle) with a two-way gaseous laser gain section incorporated in one leg. The effective laser cavity is the closed ring. Application of Equation (1) leads to the conclusion that laser oscillations in one direction around the ring will have a different frequency from those in the opposite direction when the ring is in rotation. If the oppositely directed beams are heterodyned together, the beat frequency is given by

$$\Delta\nu = \frac{4A\Omega}{L\lambda} \qquad\qquad (2)$$

3

In Equation (2), L is the cavity length (assumed the same for both oscillations), λ is the laser wavelength, and the other terms are as previously defined. Even though the fundamental laser frequency is of the order of 10^{14} Hertz while the beat frequency is of the order of a few Hertz to tens or hundreds of Hertz, heterodyne detection techniques make the beat frequency readily measurable.

2.3 Ring Interferometer Rotation Sensor

The Sagnac effect can also be used as a passive rotation sensor where the light source is external to the ring and does not change in frequency (see Figure 1). The light source is affixed to the interferometer and moves with it. This is the original configuration used by Sagnac. Michelson and Gale[4] used such an arrangement on a large scale to measure earth rotation.

Application of Equation (1) to the ring interferometer shows that there is a fringe shift (phase shift) between the two beams when the ring is in rotation as compared to when it is stationary. The fringe shift is given by

$$\Delta Z = \frac{4A\Omega}{\lambda c} .\tag{3}$$

The terms are all as previously defined. Note that in each of Equations (1), (2), and (3), Ω is the rotation rate about an axis perpendicular to the plane of the ring. Each equation could be written more generally with the term $A\Omega$ replaced by $\vec{A} \cdot \vec{\Omega} = A\Omega \cos\theta$ where θ is the angle between a unit vector normal to the ring plane and the angular velocity vector. Derivations of Equation (3) are given in the references cited above.

2.4 Fiber Ring Interferometer

The ring interferometer rotation sensor discussed in Section 2.3 is

4

interesting for its physics but had little, if any, application. Michelson
and Gale used an interferometer in the shape of a rectangle with dimensions of
640 m x 320 m to measure earth rotation; but this scarcely constitutes a prac-
tical application. With the advent of single mode fiber, the situation changed
significantly. If a single mode fiber is wound about an area A with N turns,
the fringe shift given by Equation (3) is modified to become[5]

$$\Delta Z = \frac{4A\Omega N}{\lambda c} \quad , \tag{4}$$

i.e., the effective area is N times that enclosed by the ring (see Figure 2).
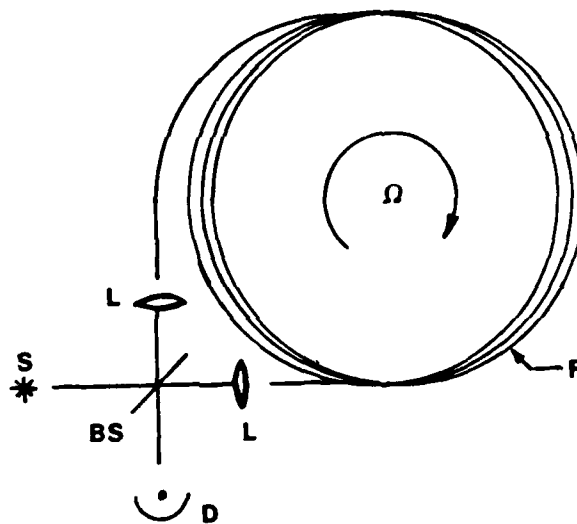
Figure 2.   Sagnac interferometer employing N turns of optical fiber resulting in
an increase in sensitivity of a factor of N over the single turn inter-
ferometer.

Because optical fibers are available in kilometer lengths, the net gain in sensitivity can be substantial. Thus it is thought that this device may have some potential in a rotation sensing application.

3.0 GEOPHYSICAL FIBER RING INTERFEROMETER CONCEPT

The GFIG concept is based on the Sagnac effect and is described below: The basic equation of the Sagnac effect is given by

$$Z = \frac{4\vec{A} \cdot \vec{\Omega}}{\lambda c} \, , \tag{1}$$

where Z is the fringe shift produced between the two counterrotating beams in the interferometer. The angular velocity (rotation rate) is $\vec{\Omega}$ and $\vec{A}$ is the area of the fiber loop. λ and c are the vacuum wavelength and free space speed of light respectively. When the area A is circular in form of radius R and the total length of the fiber is L ($2\pi RN = L$, where N is the number of loops), the equation for the fringe shift becomes

$$Z = \frac{2RL}{\lambda c} \cos\theta \, \Omega \, , \tag{2}$$

where θ is the angle between the normal to the coil and axis of rotation.

Since the purpose of the GFIG program is to develop a laser gyro capable of finding the Earth's polar axis, one can see how this is accomplished by first writing Equation (2) in the form,

$$Z = K\Omega \cos\theta \, . \tag{3}$$

The sensitivity of the interferometer with respect to pointing angle is obtained by differentiating Equation (3), i.e.,

$$\frac{dZ}{d\theta} = -K\Omega \sin\theta \quad .$$
(4)

When $\theta = \pi/2$, $dZ/d\theta$ is a maximum. Thus, in a one or two-axis GFIG, the gyro-scope will be allowed to orient itself such that one or both coils are perpendic-ular to the axis of rotation.

3.1 Gyroscope Performance Requirements

Gyroscope manufacturers conventionally express the sensitivity of their devices in terms of a drift rate (i.e., the minimum rotation rate that can be detected). Since the ultimate pointing accuracy is a function of the drift rate, it will be useful to relate these two quantities through a parametric expression. Figure 3 illustrates the geometry which allows the formulation of this relation-ship.
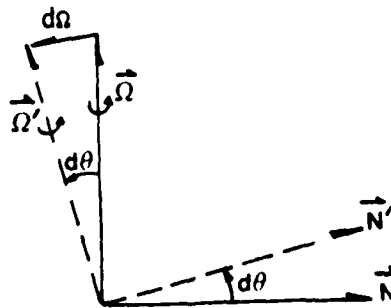
Figure 3.   Vector geometry.

7

The gyroscope is perfectly aligned whenever $\vec{N}$ and $\vec{\Omega}$ (given by the solid lines) are exactly perpendicular (note that a two-axis system is required for determing North). Any slight misalignment of the normal $\vec{N}$ away from the perpendicular to $\vec{\Omega}$ (i.e., $\vec{N} \rightarrow \vec{N}'$) results in a change in the phase difference which, in turn, can be interpreted as a change in the rotation rate from $\vec{\Omega} \rightarrow \vec{\Omega}'$. $d\Omega$ is related to $d\theta$ by

$$d\Omega = \Omega d\theta \quad . \tag{5}$$

Figure 4 illustrates the drift rate requirements as a function of the desired pointing accuracy. The curve is valid for any type of laser gyro under consideration.
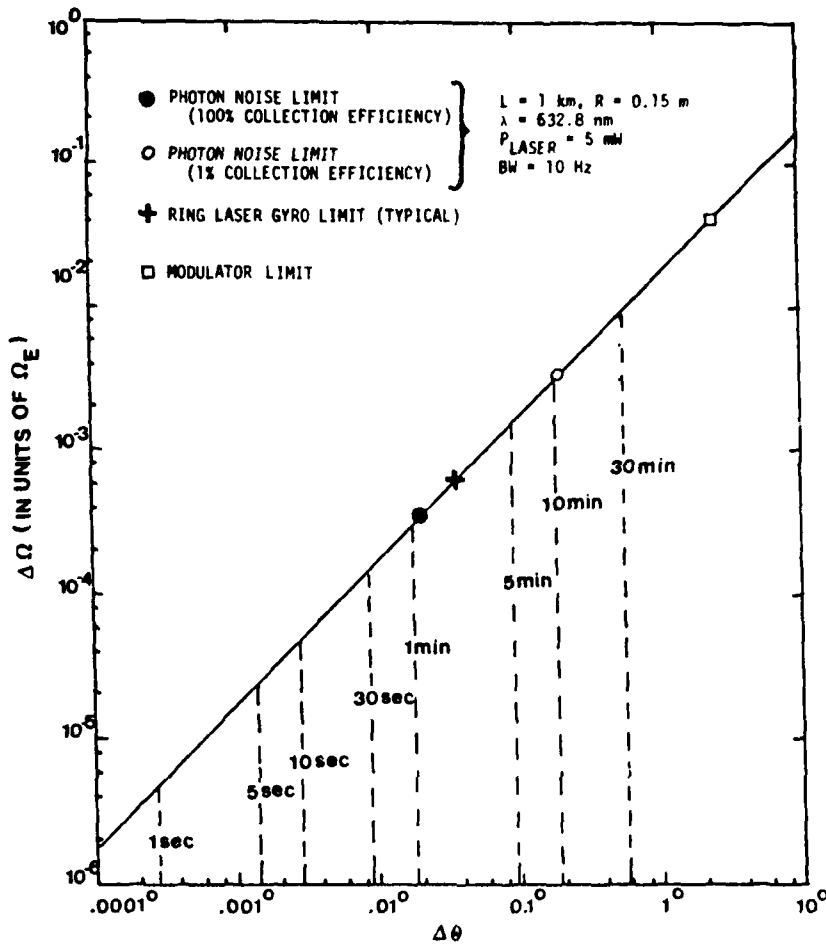
Figure 4. Drift rate requirements for indicated pointing accuracies.

4.0 PHASE BIASING A FIBER INTERFEROMETER

Rotation rate (or equivalently alignment information in the case of the GFIG) is obtained from the interferometer by a measurement of the fringe shift produced between the two counterrotating beams. The fringe shift in turn is determined from a measurement of the fringe intensity that results when the two

beams are recombined. The fringe intensity resulting from the interference of the two beams is given by

$$I = I_o[1 - m \cos(2\pi\Delta Z + \phi_B)]. \tag{1}$$

where ΔZ is the fringe shift given by Equation (2) in Section 3.0, m is the fringe visibility and ϕ_B is the phase shift between the two beams in the absence of rotation. Normally, $\phi_B = 0$. The visibility may be less than 100% due to departure from an exact 50/50 beamsplitting ratio and inequality between the fiber coupling coefficients. Although not indicated, Equation (1) may also contain DC offset terms due to: 1) detector dark current, or 2) amplifier offsets and drifts. The fringe intensity as a function of rotation rate is illustrated in Figure 5.
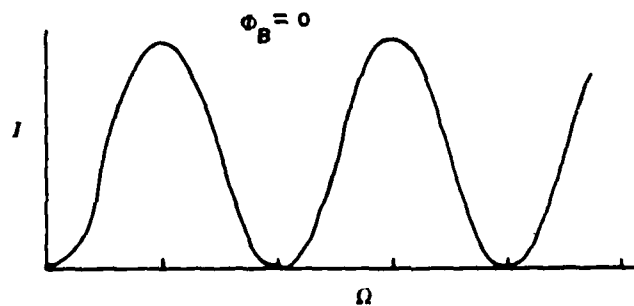
Figure 5.   Fringe intensity I vs. rotation rate Ω .

The sensitivity of a fiber interferometer gyroscope to rotation is deter-
mined by the ability to measure small changes in the intensity of the fringe
pattern. Some researchers[6] have pointed out the lack in sensitivity of this
method in the detection of low rotation rates since the slope of the I vs. Ω
curve (Figure 5) approaches zero as $\Omega \rightarrow 0$. Their solution is to impose a non-
reciprocal static phase bias, $\phi_B = \frac{\pi}{2}$, between the two counterrotating beams,
thus moving the operating point, for low rates, to the point of maximum slope
on the I vs. Ω curve (Figure 6).
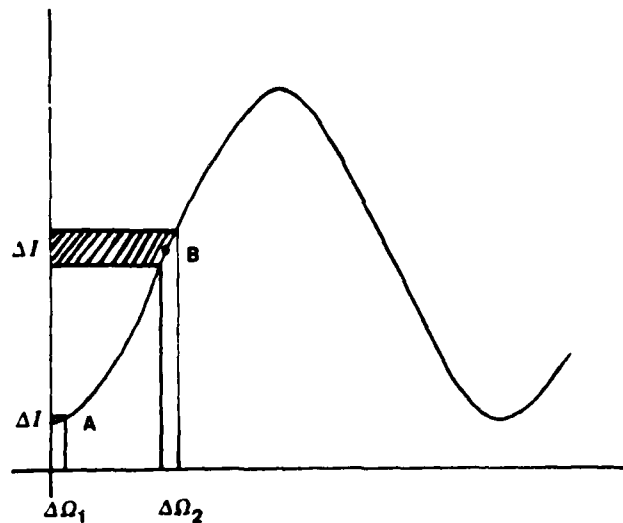
Figure 6.   Transfer function.

A = operating point with no phase offset.
B = $\pi/2$ phase offset. Most sensitive portion
        of the transfer function. $\Delta\Omega_1 = \Delta\Omega_2$

Prior to discussion of the methods by which a phase bias can be imposed on the interferometer output, it should be pointed out that analysis shows that even if a stable DC phase bias could be successfully imposed between the two counterrotating beams, the improvement would be marginal ($\sqrt{2}$ improvement). This analysis assumes the ideal case; namely that the only source of noise present in the measurement is shot noise - other sources of noise, e.g., 1/f noise in the detectors and amplifiers, Johnson noise, laser intensity fluctuations, coupling efficiency drifts (discrete component system only), birefringent changes in the optical properties of the fiber, etc., were all assumed to be negligible. Recalling that a change in rotation rate is sensed as a change in fringe intensity, the increase in the shot noise component (which goes as the square root of the fringe intensity) offsets the advantage brought about by the increased slope of the I vs. Ω curve as the bias is changed from zero to $\pi/2$. (Note: the earlier comments regarding improved sensitivity with a DC phase bias are, however, valid in the presence of noise sources other than that of shot noise -- an example of this is the large 1/f noise component inherent in transimpedance-type current-to-voltage preamplifiers. Other choices, however, do exist for detector-preamplifier combinations and signal processing for which this noise component is not a factor).

Although the application of a DC phase bias produces only a marginal increase in sensitivity, a method for the GFIG was adopted in which a phase dither is produced between the two counterrotating beams, thus allowing a means for implementing a phase-sensitive detection method that is independent of *chopping* the source laser -- a phase sensitive method based solely on chopping the source laser would not be independent of intensity drifts in the source.

Methods by which a phase bias, DC or otherwise, can be imposed, and their advantages and disadvantages are discussed in the following sections.

12

4.1 Nonreciprocal Methods

There are several methods by which a nonreciprocal DC phase bias can be generated. These involve the use of Faraday cells, misalignment of the input and output beams, phase masks, electro-optic phase shifters, and acousto-optic frequency shifters. Each of these in turn will be discussed below and the advantages and disadvantages of each will be addressed.

(a) If the input beams are intentionally misaligned as they are coupled into the fiber ends (discrete components system only), the result may be two beams propagating through the fiber in opposite directions but along nonreciprocal paths. The disadvantage of this method is that it is extremely environmentally sensitive (since the propagation is along nonreciprocal paths) and thus would be a major source of noise in any measurement.

(b) Another method that has been utilized in discrete component systems is the use of "complementary" phase masks[10]. In this method, two separate detectors are used to look at the fringe intensity in the complementary fringe patterns (each pattern is 180° out of phase with respect to the other). Instead of forming the null field as the two beams are recombined, one beam is defocussed with respect to the other, resulting in a Newton-ring type interference pattern. The zeroth-order fringe in one pattern is dark and that in the other pattern is bright. One fringe pattern is masked such that its detector sees only the central fringe and one-half of the first dark ring. The other pattern is masked so that its detector sees the complement of the other half of the .first dark ring and half of the first bright ring. The outputs of these two detectors are then differenced. It is claimed that the use of these masks is equivalent to an integration over the fringe pattern where the phase is allowed to go from zero to 180°, resulting in an output signal that is biased by nearly 90°.

(c) Another mechanical type method is to adjust the two output beams such

that there is a small tilt between them. If the beams are well collimated, a set of parallel fringes will be formed. By choosing an aperture of sufficient limiting diameter, an equivalent phase bias of $\pi/2$ can be imposed on the detector output. The best choice would be to put only one fringe in the field and choose an aperture that would cover half the fringe (i.e., from dark to bright). This method is essentially equivalent to the preceding one but is much easier to implement.

The three preceding methods, however, all suffer from the same serious drawbacks, i.e., in discrete systems there are always the problems associated with mechanical motion, vibration, thermal drift, etc. These will be manifested in the form of random phase and intensity fluctuations.

(d) A technique that has been used to unlock a ring-laser involves the use of a <u>Faraday cell</u>. In this method, biasing is achieved with an intracavity magneto-optic element surrounded by a current-carrying solenoid and situated between two orthogonally aligned quarterwave plates. It has been suggested[7-9] that the same method could be used to bias an interferometer. However, ring-laser gyro manufacturers have almost completely abandoned this technique because of the difficulty in stabilizing the bias frequency (bias phase in case of an interferometer). The stabilization problem depends on several factors including the holding of a constant solenoid current, temperature control of the magneto-optic element (since the Verdet constant is temperature dependent), and shielding against stray magnetic fields. Despite the most careful attempts to control drifts in these problem areas, success has remained elusive. Thus it does not seem appropriate to use Faraday cells for biasing a fiber interferometer gyroscope since the same problems would be encountered.

(e) Another method of utilizing nonreciprocal optical elements is based on the electro-optic effect in crystals[11,12]. In this method, a nonreciprocal

phase shift can be produced between the CW and CCW beams. Normally, these are reciprocal devices but by choosing orthogonal polarizations for the two beams, nonreciprocal operation can be achieved. However, since two different modes of polarization are being propagated thru the fiber, the effective length of the fiber can be different for each beam since the fiber is birefringent. The birefringence of these fibers can be temperature and pressure sensitive and hence, fluctuations in the nonreciprocal phase shift arise. Since these cannot be distinguished from rotational-inducted phase shifts, a large drift error would result with this method.

(f) A final method potentially capable of introducing a fixed bias phase with a very high degree of stability is based on the utilization of <u>Bragg-type</u> <u>acousto-optic frequency shifters</u>[11]. Figure 7 illustrates how these elements could be incorporated into a rotation-sensing device.
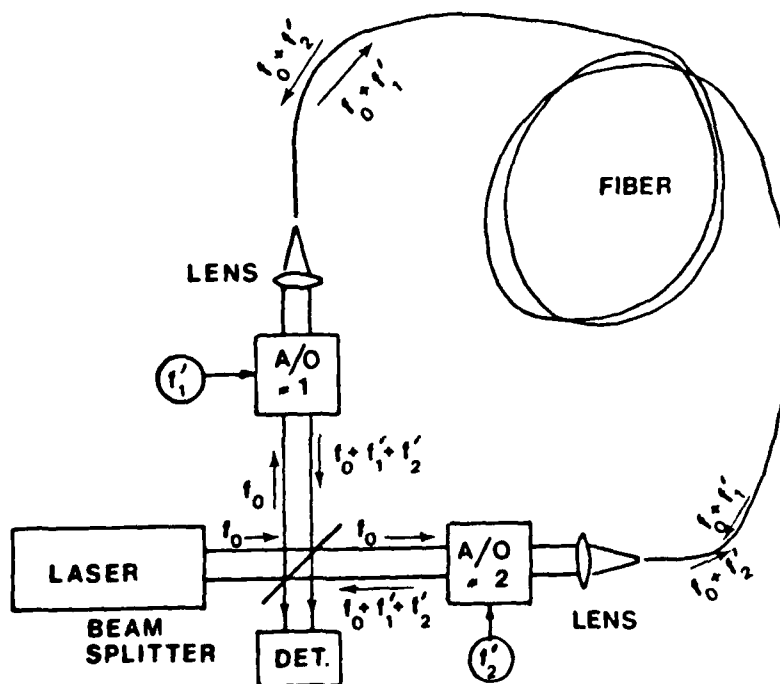
Figure 7. Schematic diagram of a system for introducing a nonreciprocal phase shift using acousto-optic frequency shifters.

As shown in Figure 7, half the light passes through A/O #1 and propagates in a CW direction along the fiber. After emerging from the other end of the fiber, it passes through A/O #2 and is reflected out to the detector by the beamsplitter. Similarly, the second half of the laser beam first passes through A/O #2 and propagates along the fiber in a CCW direction, after which it passes through A/O #1 and the beamsplitter to interfere with the CW beam. If A/O #1 is driven at frequency f_1', then the CW propagation along the fiber will be at a frequency $f_o + f_1'$ where f_o is the laser frequency. Similarly, if A/O #2 is driven at frequency f_2', then the CCW propagation along the fiber is at frequency $f_o + f_2'$. However, both beams upon exiting from the interferometer have the same frequency, $f_o + f_1' + f_2'$.

Since the frequency is different for the two beams propagating in the CW and CCW directions, they will emerge from the fiber ends with a phase difference given by

$$\Delta\phi = 2\pi\left(\frac{L_1}{\lambda_1} - \frac{L_2}{\lambda_2}\right) \quad , \tag{1}$$

where λ_1 and λ_2 are the wavelengths in the fiber and are related to the vacuum wavelengths by $\lambda_1 = \frac{\lambda_{1_o}}{n}$ and $\lambda_2 = \frac{\lambda_{2_o}}{n}$, and n is the index of refraction. The wavelengths λ_{1_o}, λ_{2_o} are related to the frequency by $\lambda_{1_o} = \frac{c}{f_1}$, $\lambda_{2_o} = \frac{c}{f_2}$ where $f_1 = f_o + f_1'$ and $f_2 = f_o + f_2'$. Upon substituting, Equation (1) becomes

$$\Delta\phi = \frac{2\pi n}{c} [f_1 L_1 - f_2 L_2] . \tag{2}$$

In Equation (2), L_1 and L_2 are, in general, unequal since in a rotating system the times required to traverse the fiber are unequal. If the fiber is rotating in a clockwise direction, L_1 and L_2 are given by

16

$$L_1 = \frac{c}{n} t_1 = \frac{c}{n} \frac{L}{(\frac{c}{n} - R\Omega)}$$

<div align="right">(3)</div>

$$L_2 = \frac{c}{n} t_2 = \frac{c}{n} \frac{L}{(\frac{c}{n} + R\Omega)} \; ,$$

where R is the fiber coil radius and Ω is the rotation rate.

Upon substituting into Equation (2), the phase difference becomes

$$\Delta\phi = 2\pi L \left| \frac{\frac{c}{n}(f_1 - f_2) + R\Omega(f_1 + f_2)}{(\frac{c}{n})^2 - R^2\Omega^2} \right|$$

<div align="right">(4)</div>

In most cases, $R\Omega \ll \frac{c}{n}$. Therefore,

$$\Delta\phi = \frac{2\pi nL}{c} [(f_1 - f_2) + \frac{nR\Omega}{c} (f_1 + f_2)] \quad .$$

<div align="right">(5)</div>

The first term in the bracket of Equation (5) represents the bias phase shift and is given by

$$\Delta\phi_B = \frac{2\pi nL}{c} (f_1 - f_2) = \frac{2\pi nL}{c} (f_1' - f_2') \quad ,$$

<div align="right">(6)</div>

while the last term is the rotation-induced phase shift.

The bias angle, $\Delta\phi_B$, can be adjusted to any value according to the length L of the fiber by a suitable choice of the frequency difference, $f_1' - f_2'$, of the acousto-optic modulator drive frequencies. In particular, if both frequencies

<div align="center">17</div>

are derived from the same oscillator and frequency doublers (or triplers, etc.) are used to generate the difference frequency, a very high degree of bias angle (phase) stability can be achieved.

Of all the methods enumerated above for producing a nonreciprocal DC phase bias, only the last method (acousto-optic frequency shifters) seems to offer potential. Not only is this method the only one capable of producing a stable DC phase bias (whenever crystal oscillators or stable frequency synthesizers are used), it is only one capable of producing a bias that is accurately known. An accurate and precisely known bias (with as many significant figures as required) is necessary since any uncertainty here would contribute to the total drift rate error. Furthermore, if properly used (e.g., in a phase nulling mode), this technique can provide a direct readout of rotation rate (via Equation (6)) that is independent of a fringe intensity measurement.

4.2 Reciprocal Methods

There are two methods by which the optical path length in each direction can be changed by the same amount (assuming the same polarization state). Since the paths are reciprocal in both directions, no advantage is gained by the incorporation of this type of phase shifter unless somehow a nonreciprocal phase shift can be induced. Such a means exists if the phase can be modulated. The modulation method will be discussed in the next section.

It will suffice to say that one of the methods is based on the photo-elastic effect in which a small change in the refractive index can be obtained by applying either a transverse or longitudinal strain to the fiber via pizeo-electric elements. However, the application of mechanical stress may produce undesirable side effects on the birefringent properties of the fiber. Therefore, it was felt that this method was not a viable one for this application,

although it may fulfill some requirements in communications systems.

The other method is based on the usage of an electro-optic (Pockels-type) phase shifter. This is the method UURI has adopted and will be discussed in the following section.

4.3 Nonreciprocal Phase Modulation

Several of the methods discussed above can be used in a nonreciprocal phase modulation type of scheme. The advantage of phase modulation lies within the techniques that can be utilized in the signal processing. Signal processing will be discussed in Section 6.

Two of the methods previously discussed can be excluded outright. These are the ones utilizing the nonreciprocal Faraday cell and the reciprocal photoelastic effect.

The third method involving acousto-optic frequency shifters has some potential in an integrated optical system, but not in a discrete component system. In the A/O method[11,13], the frequency of one of the oscillators driving an acousto-optic frequency shifter is allowed to vary in a manner such that the phase bias is modulated between the extremes of zero and 90°. The method for extracting rate information is the same as that for the electro-optic method, which will be discussed in subsequent sections.

The utilization of A/O frequency/phase modulation in a discrete system is limited by the fact that this type of phase modulator inherently dithers the beam across the fiber ends, thus introducing an intensity modulation that is independent of any rotation-induced modulation of the interferometer output. This effect was evaluated experimentally and will be discussed in Section 8.

The method adopted for the GIIG is based on the electro-optic (Pockels-type) phase modulator. Normally, these are reciprocal devices. However, with

19

a phase modulation timed according to the propagation time through the fiber, a nonreciprocal phase shift can be introduced between the two beams. In this method, a single phase modulator is inserted into one arm of the interferometer (Figure 8).
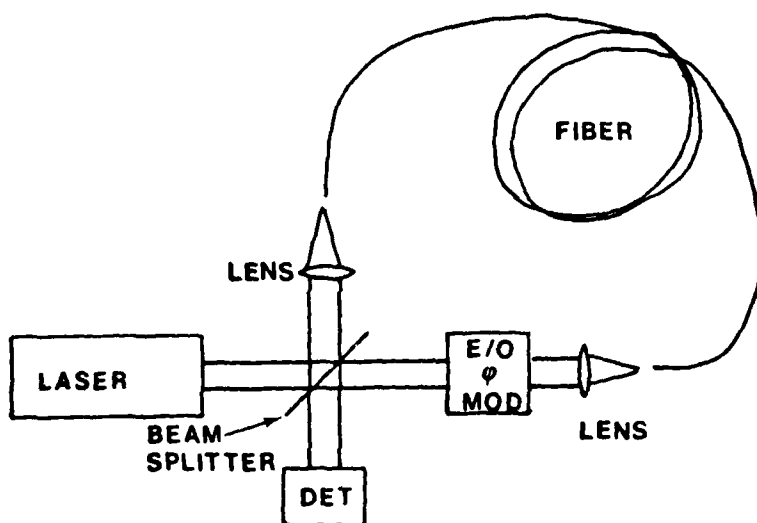
Figure 8. Schematic diagram of a system for introducing a nonreciprocal phase shift using an electro-optic phase modulator.

Figure 9 illustrates the manner in which modulation techniques can be used to produce a nonreciprocal phase shift between the two counterrotating beams.

a) Travel Time in Fiber (1 KM)

0   5 µsec

b) Sinewave phase modulation of period $2T_D$

$\pi/4$

$-\pi/4$

T_D $2T_D$ $3T_D$

c) Phase modulation on the CW beam for constant angular rotation rate giving a phase shift of ϕ_r (after emerging from fiber)

$\pi/4 + \frac{\phi_r}{2}$

$-\pi/4 + \frac{\phi_r}{2}$

T_D $2T_D$ $3T_D$

$\pi/4 - \frac{\phi_r}{2}$

d) Phase modulation on CCW beam (after emerging from fiber)

$-\pi/4 - \phi_r/2$

T_D $2T_D$ $3T_D$

e) Intensity modulation observed at the detector output

$1 +$

A

B

$\phi_r = 0$

T_D $2T_D$ $3T_D$
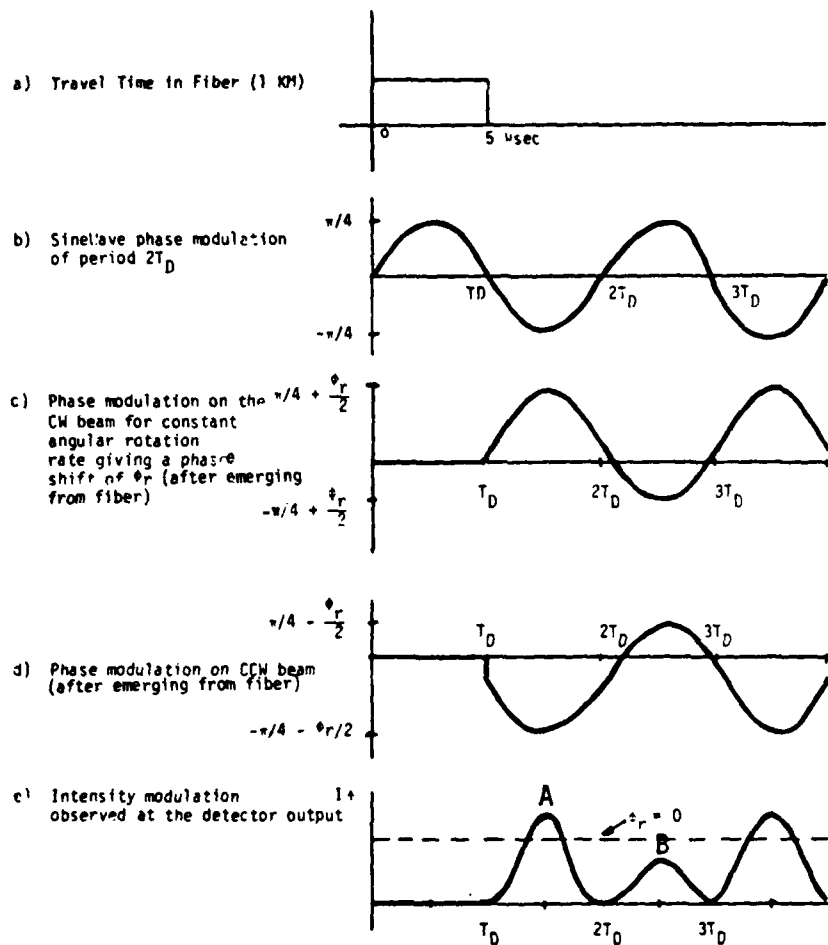
Figure 9. Timing sequence for producing nonreciprocal
phase shifts using a reciprocal electro-optic
phase modulator.

In Figure 9b, a sinewave phase modulation having an amplitude of $\pi/4$ radians and a period $2T_D$ (T_D = propagation time in the fiber) is applied to the electro-optic phase modulator. Each beam upon emergence from the fiber, has impressed on it a phase shift of $\pi/4$ radians (in addition to any rotational-induced phase shift). However, this phase shift has an opposite sign for each beam due to the fact that

21

the sign of the impressed phase changes for the beam that entered the fiber from the opposite end (assuming that the period of the phase modulation is twice that of the propagation period in the fiber). Hence, in the absence of rotation, the two beams emerge from the fiber with a phase difference equal to twice the instantaneous phase shift introduced by the modulator. Thus, if the amplitude of the modulator is $\pi/4$ radians, the maximum phase difference between the two beams is $\pi/2$. In the presence of rotation, the instantaneous phase shift may be written as

$$\phi = \phi_r + \frac{\pi}{2} \sin (2\pi f_m t) \qquad (7)$$

where ϕ_r is the rotation-induced phase shift and f_m is the modulation frequency. The intensity in the resultant fringe pattern may be written as

$$I = I_0 [1 - m \cos (\phi_r + \frac{\pi}{2} \sin 2\pi f_m t)] \qquad (8)$$

Figure 9e is a plot of intensity modulation in the presence of rotation. In a North-seeking application, the gyroscope is allowed to align itself such that the component of the earth rotation rate along the normal to the coil becomes zero. Thus, the intensity maxima, A and B, become equal when the coil is perpendicularly aligned to the polar axis.

5.0 SIGNAL PROCESSING REQUIREMENTS

Extraction of rate information from the interferometer is obtained by a measurement of the fringe shift produced between the two counterrotating beams. The fringe shift in turn is determined from a measurement of the fringe intensity

that results when the two beams are recombined. This section outlines the minimum fringe shift detectibility requirements and the resolution required on the the fringe intensity measurement. It also addresses the amplitude and frequency stability requirements on the phase modulator. Additionally, the frequency stability requirements of acoustic-optic frequency shifters will be considered.

5.1 Minimum Fringe Shift Detectibility Requirement

The equation for the fringe shift may be written as

$$\Delta Z = \frac{2RL}{\lambda c} \Delta \Omega \; . \tag{1}$$

where $\Delta \Omega$ is the component of Earth's rotation rate along the normal to the fiber optic coil. Recalling that in the GFIG application the coils are allowed to orient themselves perpendicular to the rotation axis, $\Delta \Omega$ may be written as

$$\Delta \Omega = \Omega_E \Delta \theta \; . \tag{2}$$

where $\Delta \theta$ is the uncertainty in the pointing angle of the fiber optic coil. Combining Equations (1) and (2), the fringe shift may be expressed as

$$\Delta Z = \frac{2RL}{\lambda c} \Omega_E \Delta \theta \; . \tag{3}$$

The minimum fringe shift detectibility has been calculated as a function of alignment error for a 30 cm diameter coil having a fiber length of 1 km. These results are illustrated in Figure 10.
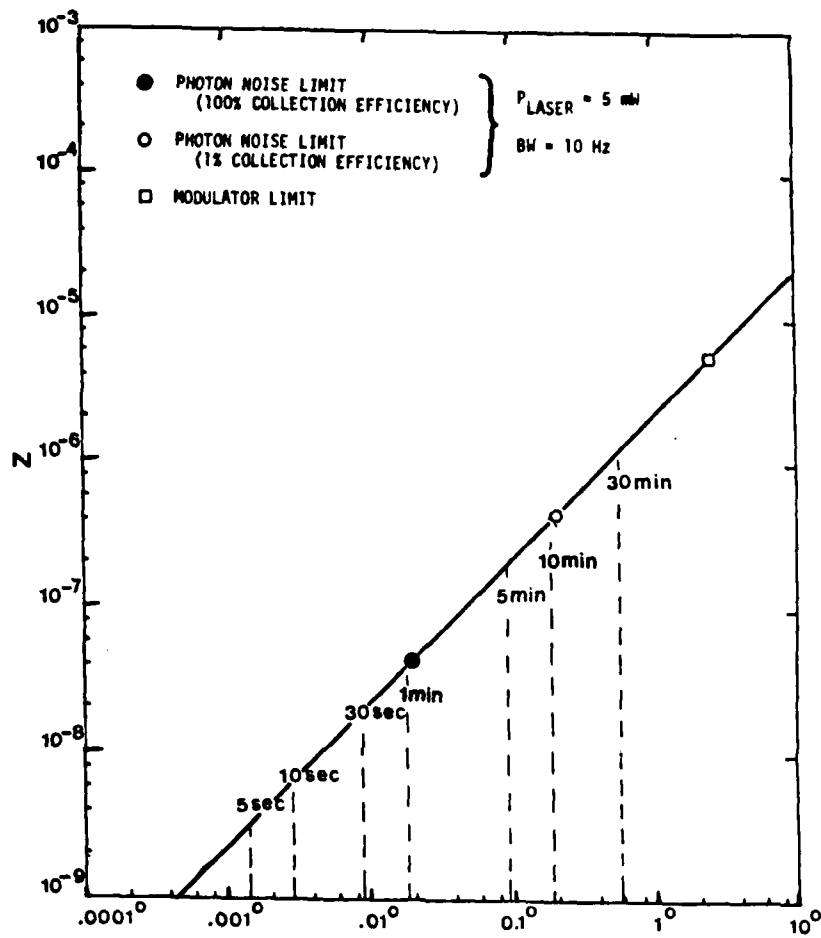
Figure 10.   Fringe shift Z produced by indicated pointing
               error $\Delta\theta$.   L = 1 km, R = 0.15 m and λ = 632.8 nm.

5.2 Resolution Requirements on the Fringe Intensity Measurement

With phase modulation the output of the interferometer is given by

$$I = I_o[1 - m \cos(\phi_r + \frac{\pi}{2} \sin 2\pi f_m t)] \tag{4}$$

where ϕ_r is the rotation-induced phase shift and f_m is the modulation frequency.

24

Figure 9e is a plot of this function in the presence of rotation. The maxima, A and B, become equal in the absence of rotation or else when the coil is aligned perpendicularly to the axis of rotation.

The alignment sensitivity therefore lies in the ability to successfully differentiate small differences in the intensity maxima. These maxima are seen to occur at times $T_D/2$ and $3T_D/2$ and are given by

$$I(T_D/2) = I_o[1 + m \sin \phi_r] ,$$

$$(5)$$

$$I(3T_D/2) = I_o[1 - m \sin \phi_r] .$$

The difference in the two maxima is therefore

$$\Delta I = 2mI_o \sin \phi_r \qquad . \qquad (6)$$

Now,

$$\phi_r = \frac{4\pi LR}{\lambda c} \Omega_E \cos\theta = K \cos\theta \qquad (7)$$

where θ is the angle between the rotation axis and the normal to the coil. If the error angle is given by

$$\Delta\theta = \frac{\pi}{2} - \theta , \qquad (8)$$

then with the aid of Equations (7) and (8), Equation (6) becomes

$$\Delta I = 2mI_o \sin(K \sin \Delta\theta). \qquad (9)$$

With a fringe visibility of 100%, the fractional change in fringe intensity becomes

$$\frac{\Delta I}{I_o} = 2 \sin(K \sin \Delta\theta). \qquad (10)$$

In Equation (10), I_o is the intensity of each of the maxima in the absence of rotation. Figure 11 illustrates the resolution that is required in a measurement of fringe intensity as a function of the angular pointing error.
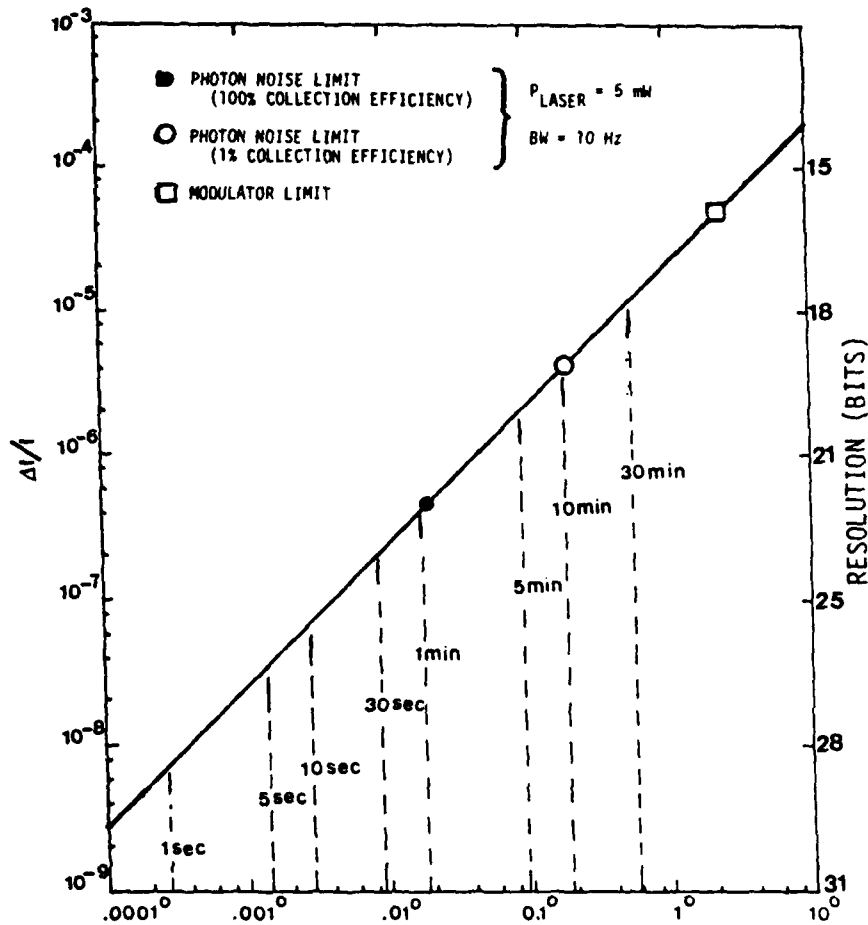
Figure 11. Fractional change in fringe intensity $\Delta I/I$ vs. pointing error $\Delta\theta$. The bias angle is $\pi/2$, $L = 1$ km, $R = 0.15$ m and $\lambda = 632.8$ nm.

5.3 Stability Requirements on Electro-Optic and Acousto-Optic Phase Shifters

The success of any type of interferometer device used to extract rate information from the measurement of a fringe shift depends not only upon the resolution in the measurement of fringe intensity but also upon the elements inserted into the optical train-elements that are required to enhance the sensitivity of the basic device itself for low rate applications.

The necessity of introducing a nonreciprocal phase bias was discussed in Section 4.0. Two types of devices described in that section appeared to offer some potential. These were the electro-optic phase shifter and the acousto-optic frequency (phase) shifter.

A serious limitation of the A/O device (with modulation) in a discrete component system was pointed out in Section 4.3. However, it could be used in a discrete system requiring only a DC phase bias or else in an integrated system (with phase modulation) in which the effect of beam motion or dither is expected to be far less serious. In Section 4.1, the nonreciprocal phase shift was found to be

$$\Delta\phi_B = \frac{2\pi nL}{c} (f_1' - f_2') , \qquad (11)$$

where f_1' and f_2' are the frequencies of the oscillators driving the A/O frequency shifters. The equivalent fringe shift is given by

$$\Delta Z = \frac{nL}{c} (f_1' - f_2') . \qquad (12)$$

If a phase shift of $\pi/2$ is desired, then the frequency difference that is required becomes

$$f_1' - f_2' = \frac{c}{4nL} , \qquad (13)$$

and for a 1 km fiber is 51.44 KHz. The frequency stability requirements can be obtained by equating ΔZ in Equation (12) to Equation (3), i.e.,

$$\Delta Z = \frac{nL}{c} \Delta f = \frac{2RL}{\lambda c} \Omega_E \Delta\theta . \qquad (14)$$

28

Thus,

$$\Delta f = \frac{2R\Omega_E \Delta\theta}{n\lambda} \qquad (15)$$

These results are illustrated in Figure 12 where R = 15 cm, n = 1.458, and
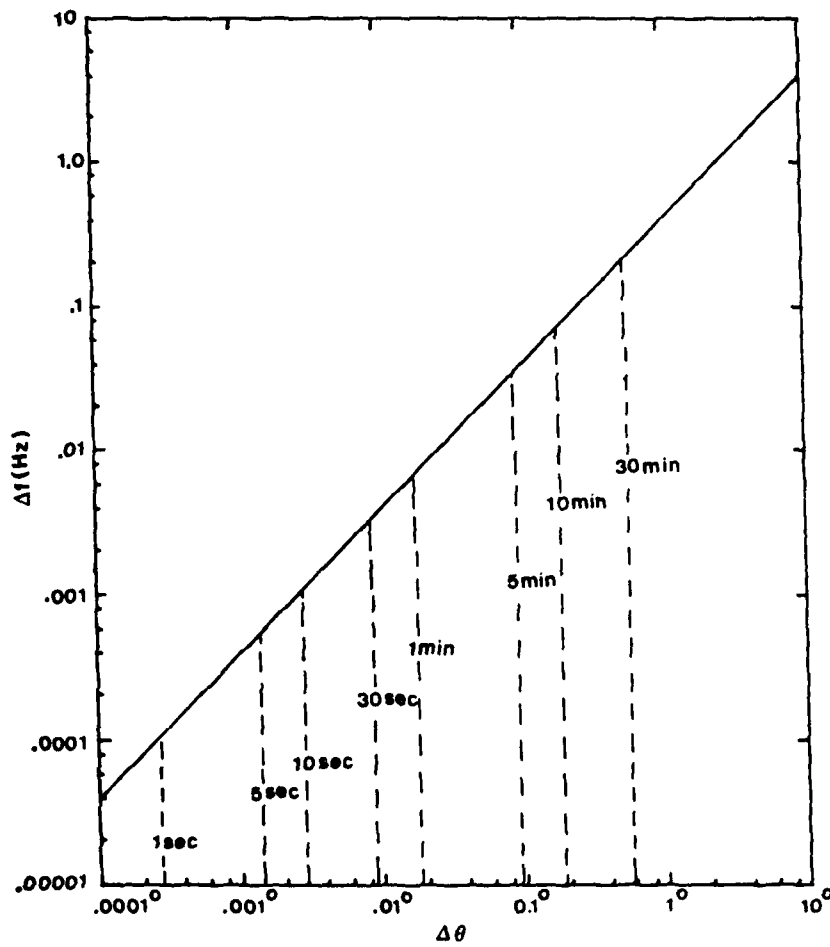
λ = 632.8 nm.

Figure 12.   A/O oscillator frequency stability required for indicated pointing error $\Delta\theta$. L = 1 km, R = 0.15 m, and λ = 632.8 nm.

Acousto-optic modulators generally require a drive frequency in the range of 50 - 100 MHz. With crystal oscillators or modern frequency synthesizers having stabilities on the order of one part in 10^{11} - 10^{13}, pointing accuracies on the order to 0.1 sec to 10 sec could, in principal, be achieved with this method if random phase fluctuations from the A/O devices were the only source of noise and the problem with resolution in the fringe intensity measurement was not a factor.

With an electro-optic phase modulator, the frequency stability requirements are even less severe. Assume for the moment that the amplitude of the wave form driving the modulator is a constant. Let the phase modulation be

$$\phi = \frac{\pi}{4} \cos(2\pi f_m t) \quad , \tag{16}$$

where $f_m = \frac{1}{T_m} = \frac{1}{2T_D}$. T_D is the propagation time in the fiber. The phase that is imparted to the wave that enters the fiber end from the arm in which the modulator is situated is

$$\phi_i = \frac{\pi}{4} \quad . \tag{17}$$

Assume now that the frequency of the modulator has changed by an amount Δf_m. The phase is then

$$\phi = \frac{\pi}{4} \cos[2\pi(f_m + \Delta f_m)t] \quad . \tag{18}$$

The phase of the wave that entered the fiber from the opposite direction, after time T_D, is therefore

$$\phi_f = \frac{\pi}{4} \cos[2\pi T_D(f_m + \Delta f_m)]$$

(19)

$$= -\frac{\pi}{4} \cos 2\pi T_D \Delta f_m \quad .$$

The phase difference, $\Delta \phi$, between the two interfering waves is

$$\Delta \phi = \phi_i - \phi_f = \frac{\pi}{4} (1 + \cos 2\pi T_D \Delta f_m) \quad . \tag{20}$$

If the frequency were constant, $\Delta \phi$ would just be $\pi/2$. The random phase error due to frequency drift is

$$\Delta \phi_R = \frac{\pi}{2} - \frac{\pi}{4} (1 + \cos 2\pi T_D \Delta f_m)$$

(21)

$$= \frac{\pi}{4} 2 \sin^2 \frac{2\pi T_D \Delta f_m}{2} \quad .$$

Since $T_D \Delta f_m \ll 1$, Equation (21) may be written as

$$\Delta \phi_R = \frac{\pi^3}{2} (\Delta f_m T_D)^2 \tag{22}$$

$$\approx \frac{\pi^3}{8} \left(\frac{\Delta f_m}{f_m}\right)^2 \quad . \tag{22}$$

In terms of a random fringe shift,

$$\Delta Z_R = \frac{\Delta \phi_R}{2\pi} \approx \frac{\pi^2}{16} \left(\frac{\Delta f_m}{f_m}\right)^2 . \tag{23}$$

Equating this result to Equation (3), i.e.,

$$\frac{\pi^2}{16} \left(\frac{\Delta f_m}{f_m}\right)^2 = \frac{2RL}{\lambda c} \Omega_E \Delta\theta \quad . \tag{24}$$

Thus,

$$\Delta\theta = \left(\frac{\pi^2 \lambda c}{32\ RL\Omega_E}\right) \left(\frac{\Delta f_m}{f_m}\right)^2 . \tag{25}$$

Figure 13 illustrates the pointing accuracy that could be achieved if frequency stability was the only problem encountered in the measurement.
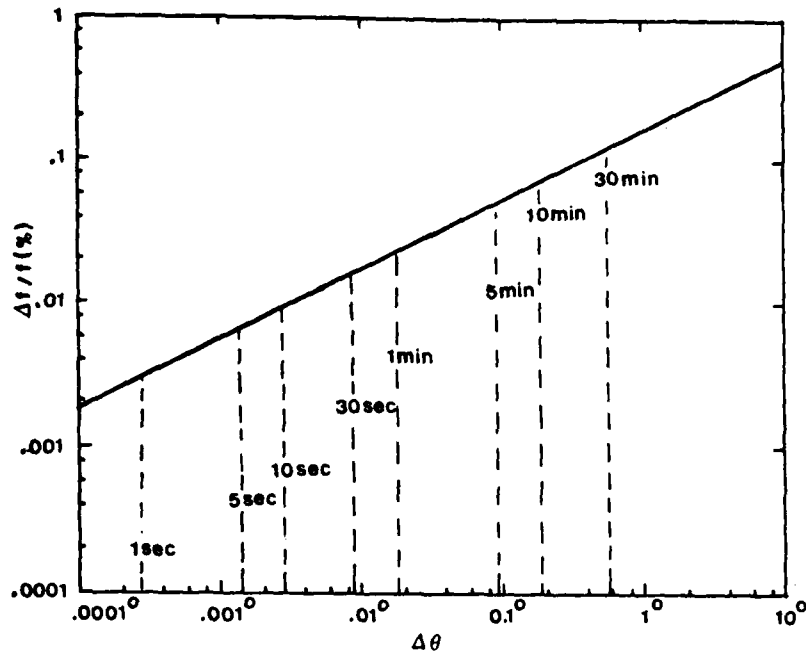
Figure 13.   E/O oscillator frequency stability required for
             indicated pointing error $\Delta\theta$.   L = 1 km, R = 0.15 m,
             λ = 632.8 nm.

A more serious problem with the electro-optic phase modulator is that asso-
ciated with the amplitude stability requirement on the drive oscillator.   In
order to assess the effect that amplitude fluctuations have on the pointing
accuracy, it is recalled that the phase shift is directly proportional to the
applied voltage, i.e.,

$$\phi = KV . \tag{26}$$

Thus a change in the applied voltage produces a fractional change in the phase
shift by an amount

$$\frac{\Delta\phi}{\phi} = \frac{\Delta V}{V} \quad .$$

(27)

Since the bias is at $\pi/2$,

$$\Delta\phi = \frac{\pi}{2}\frac{\Delta V}{V} \quad .$$

(28)

In terms of the fringe shift,

$$\Delta Z = \frac{\Delta\phi}{2\pi} = \frac{\Delta V}{4V} \quad .$$

(29)

Equating Equation (29) to Equation (3) results in an uncertainty in the pointing angle of an amount

$$\Delta\theta = \frac{\lambda c}{8RL\Omega_E}\frac{\Delta V}{V} \quad .$$

(30)

Figure 14 illustrates the pointing accuracy that can be achieved in the presence of amplitude fluctuations.

34
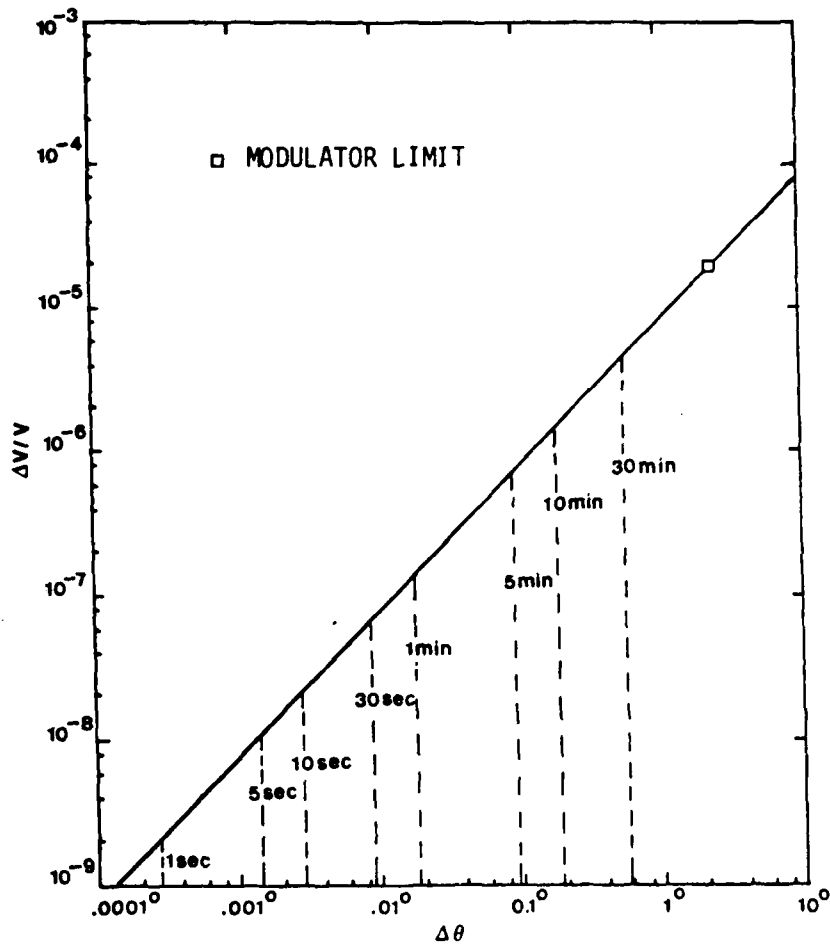
Figure 14. Electro-optic modulator drive voltage stability
requirements ΔV/V vs. pointing error angle Δθ.
L = 1 km, R = 0.15 m and λ = 632.8 nm.

The amplitude noise characteristics of the drive oscillator used in the GFIG
(0.002%) limit its performance to a 2° pointing accuracy. The 0.002% amplitude
noise seems to be quite creditable for a device of this type. Some improvement
could be expected by adding high-pass filters to the output of the oscillator.
This improvement would only be marginal and would likely be substantially less
than an order of magnitude.

A far more serious problem with the electro-optic phase modulation scheme than those discussed above occurred when the GFIG was assembled and evaluated. This concern will be addressed in Section 8.1.

6.0 SIGNAL PROCESSING METHODS

Several methods for the extraction of rate information from the resultant phase-modulated signal (Figure 9e) were evaluated. These included two sample and hold methods, a spectrum analyzer technique, and the synchronous detection method that was finally adopted. A brief description of each of these methods is given in the following sections.

6.1 Peak Detector/Sample and Hold Methods

The first two methods considered were based on sample and hold techniques. Figure 15 is a block diagram of the signal processing electronics and Figures 16 to 17 illustrate the timing sequence.
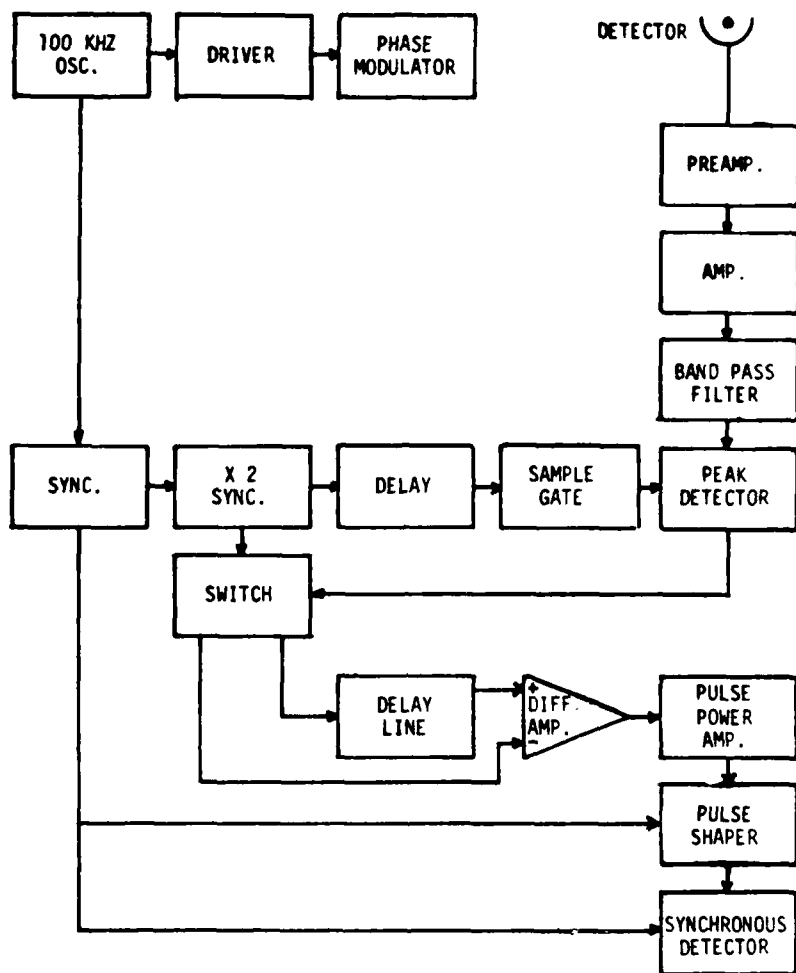
Figure 15.   Block Diagram of GFIG Electronics.

37
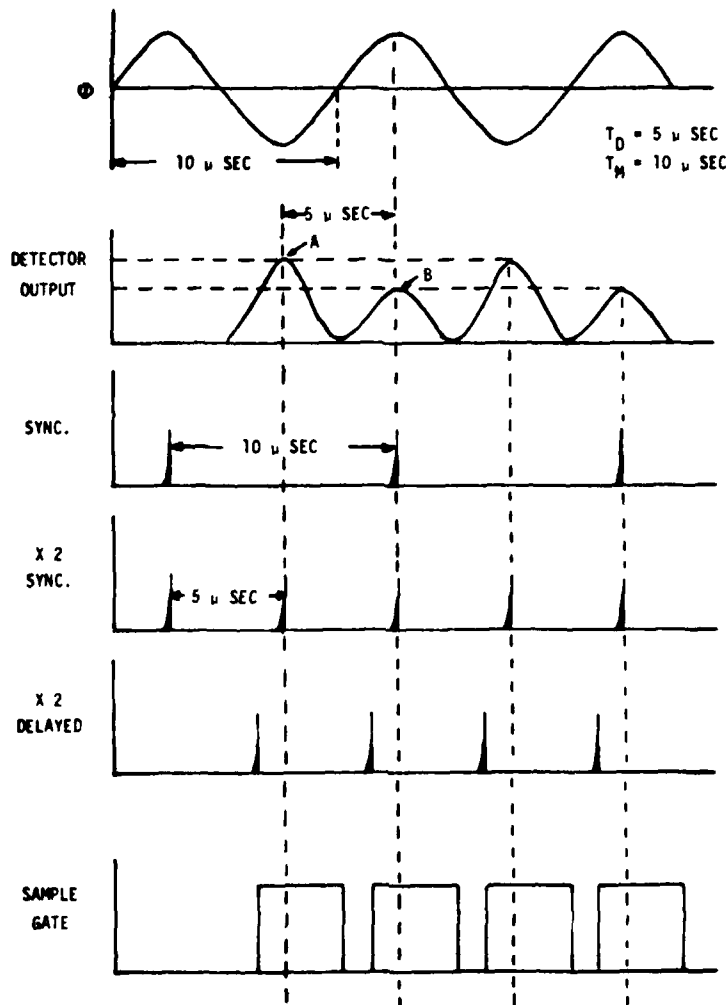
Figure 16. GFIG Timing Sequence. T_D is the delay time in the fiber and T_M is the period of the phase modulation.

38
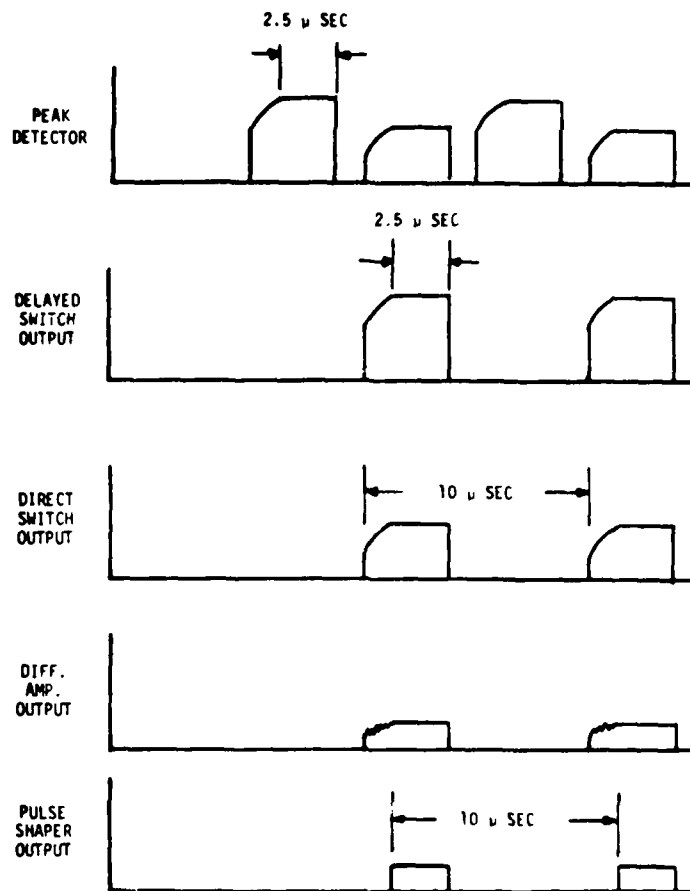
Figure 17.   GFIG Timing Sequence.

Rate information is contained in the two maxima of the detector output. Speci-
fically, the difference in the two maxima contains all the information that is
required. Due to the high data rate and resolution that is required in the mea-
surement, any technique based on digitization of the detector output can be ruled
outright. The key to a successful measurement therefore seems to lie in the
analog domain (at least in the initial stages). The method of Figure 15 is

based on a technique that allows the difference signal to be formed in the analog domain. First, a gated peak detector with a hold circuit is allowed to sample the two maxima. Next, the signal is routed to a gated switch with two outputs. Each output has been gated so that only alternate sample pulses appear on each line. Thus, each output consists of a series of pulses related to only one of the two maxima. Finally, one pulse train is delayed with respect to the other and the difference signal is formed by a differential amplifier. With some minor pulse shaping, the signal is now ready for processing by a synchronous detector.

A major problem with this technique is the delay line. The characteristics of a wide variety of delay lines, including co-axial, lumped and distributed constant, active, etc., were evaluated. All suffered greatly from the problem of pulse distortion; so much in fact that this method had to be dropped.

Another method allowing for the formation of an analog difference signal utilizing peak detection and sample and hold techniques was also investigated. Figure 18 is a block diagram of the signal processing electronics and Figure 19 illustrates the corresponding timing sequence.
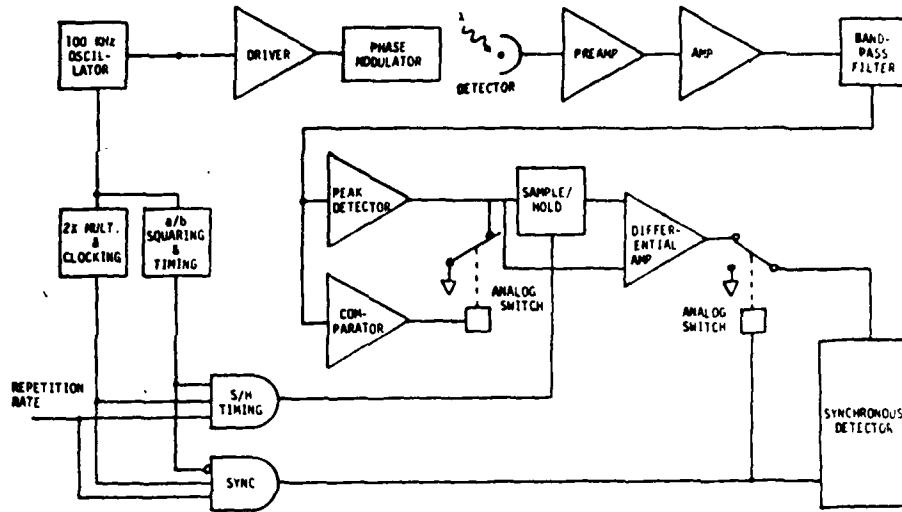
Figure 18.   Block Diagram Phase One electronics.
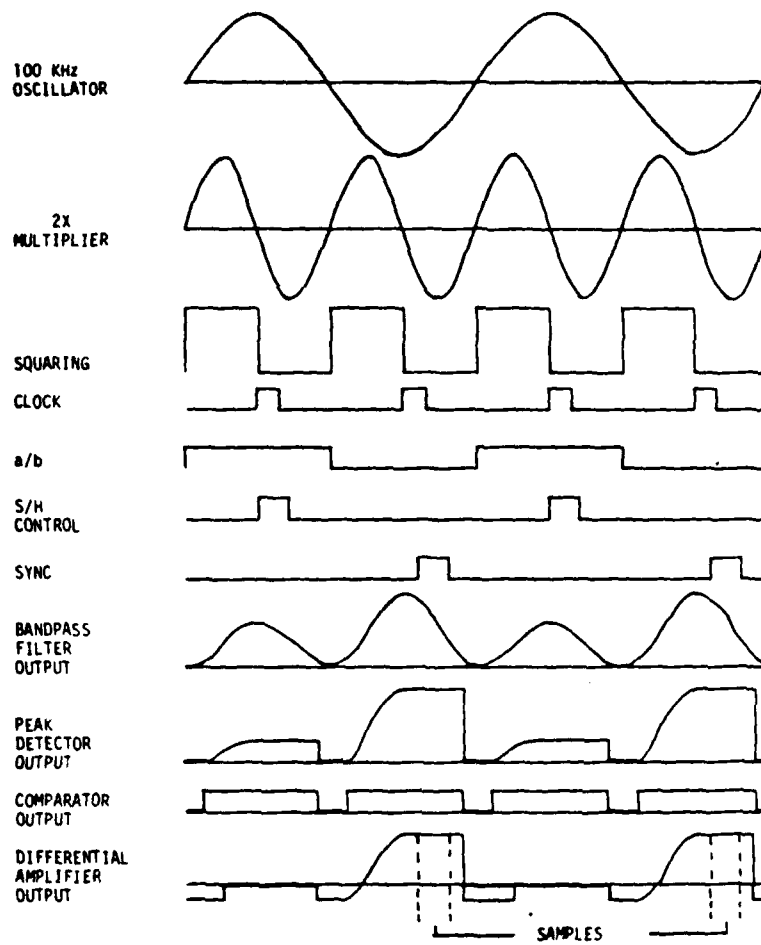
Figure 19. Timing diagram.

Basically, the technique is similar to the preceding one but delay lines have been avoided. This technique was likewise abandoned, as was the preceding one. The difficulty with this method, while not apparent, is with the sample and hold circuits. Because of the relatively long length of time required to hold the peak value of the fringe intensity, it was felt that this method was not a viable one since some drooping of the pulse was likely to occur.

6.2 Spectrum Analyzer Method

Upon examination of Figure 9e, it is seen that the amplitude of the phase-modulated signal contains two dominant frequency components. These are the fundamental of the modulation frequency and its second harmonic. Rate information is contained in the fundamental or first harmonic. The GFIG is aligned whenever the amplitude of the first harmonic goes to zero.

Another means of signal processing is therefore to examine the power spectrum of the output of the detector. This method is probably the most attractive one available since not only is it a sensitive one but it does not operate on the detector output in a deleterious manner. However, it was not adopted for the GFIG due to funding and equipment limitations.

6.3 Synchronous Detection Method

The method finally adopted for the GFIG was a synchronous detection method using a lock-in analyzer. This method is essentially the same as the one just discussed. By locking in on that frequency component (the first harmonic that contains the rate information) synchronous with the reference signal, a measure of the rotation rate can be obtained from the strength of that component. In a North-seeking application, the gyro is allowed to align itself until the signal is nulled.

43

The sensitivity of this method is limited primarily by the 2nd harmonic rejection capabilities of the lock-in analyzer and the bandpass filter. Most commercial lock-in analyzers have a 2nd harmonic rejection ratio of about -55 dB. This, in conjunction with the rejection capabilities of the bandpass filter used in the GFIG, provide a total rejection ratio of about -97 dB. The Fourier spectrum of the detector output has been calculated for a range of rotation rates. The degree of 2nd harmonic rejection required for a given pointing accuracy is illustrated in Figure 20.
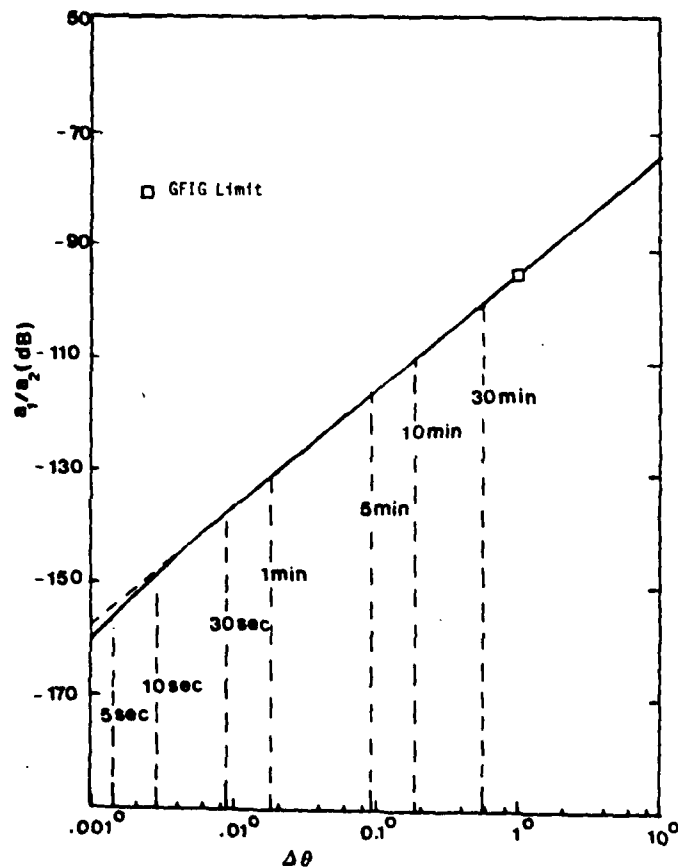
Figure 20.   First harmonic/second harmonic ratio.

The GFIG is currently limited to about a 1° pointing error. Some improvement (approx. 20 dB or less) could of course be obtained with better filtering, thus providing a pointing accuracy of about 0.1°. In view, however, of the limits that the modulators places on the pointing accuracy (Section 5.3 and 8.1), such a step is not required.

7.0 GFIG CONFIGURATION

The final configuration for the Phase I GFIG North-seeker was based upon the requirements outlined in Sections 4, 5, and 6 of this report. Reduced to essentials, the GFIG is a discrete (optical) component system utilizing an electro-optic phase modulation technique to enhance sensitivity and a synchronous detection method for the extraction of rate information.

Figure 21 is a block diagram of the GFIG optical configuration.
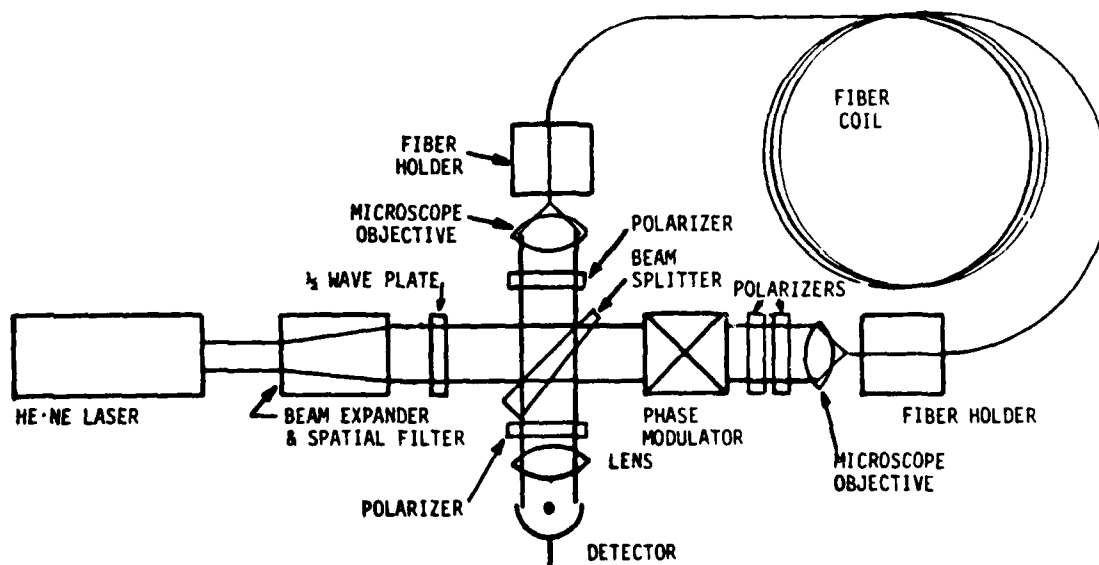
Figure 21. Optical configuration of the GFIG fiber interferometer.

The He-Ne source beam is spatially filtered and expanded up to 6-7 mm diameter. A half-wave plate is used to orient the plane of polarization so that it lies along the principal axis of the phase modulator. The polarizers immediately adjacent to the focussing lenses are used to orient the polarization vectors of the CW and CCW beams entering the fiber. The polarization vectors of these two beams are aligned along the principal axes of the two fiber ends. This requirement is necessary since it has been found that the polarization of the electromagnetic wave in the fiber is not, in general, preserved. However, polarization can be preserved if the input beam is polarized in a direction along one of the principal birefringent axes of the fiber. The function of the polarizer adjacent to the phase modulator is to orient the plane of polarization of the clockwise beam emerging from the fiber along the principal axis of the phase modulator.

Although the Phase I GFIG design was based on a 1 km long, 30 cm diameter fiber optic coil, the final configuration utilized a 1.57 km long, 1 m diameter coil. This was necessitated by the delay in delivery of the fiber from the manufacturer. Also, because of its size and length, a factor of 5 improvement in sensitivity could be expected. Figure 22 is a photograph of the completed GFIG and Figure 23 is a block diagram of the signal processing electronics used in the evaluation.
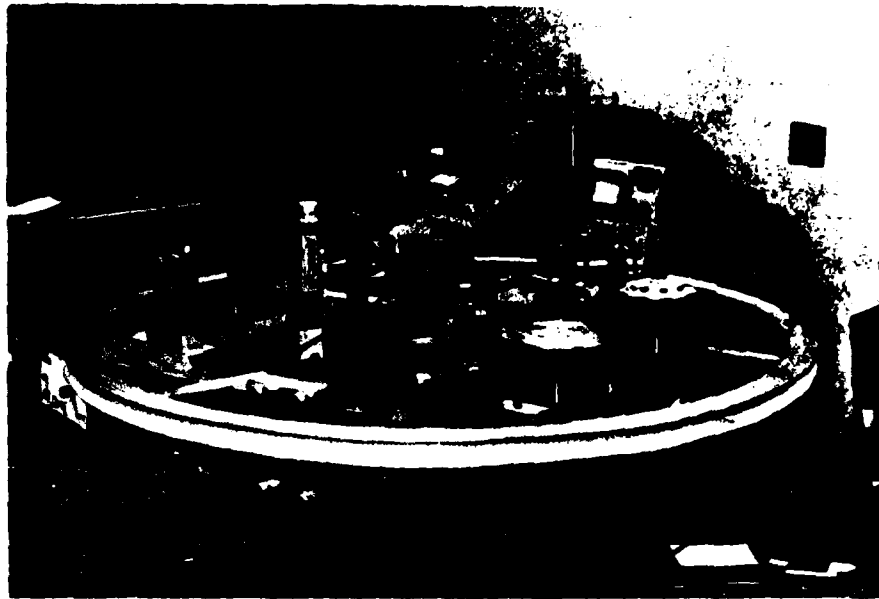
Figure 22.   Photograph of GFIG.

47
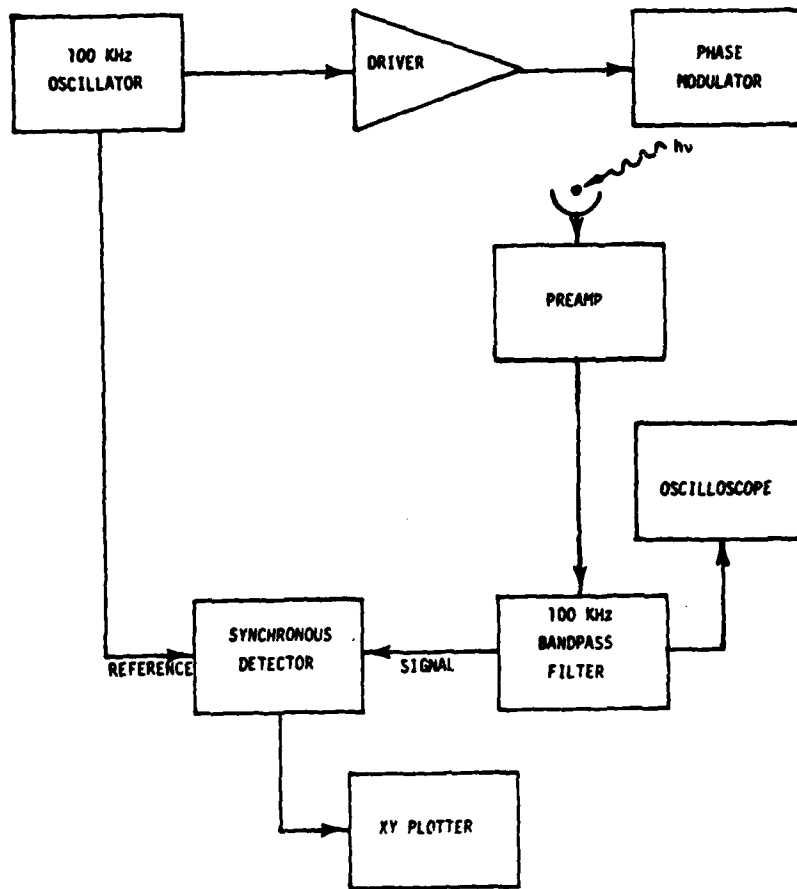
Figure 23. Block diagram of GFIG electronics.

8.0 PERFORMANCE EVALUATION

The limiting pointing accuracy of the GFIG has thus far been addressed in terms of the amplitude and frequency stability requirements on the electro-optic and acousto-optic elements used to provide phase modulation (Section 5.3) and on the second harmonic rejection capabilities of the lock-in analyzer (Section 6.3). In those sections, it was pointed out that some improvement could be expected with selective filtering, but that any improvement would be of

marginal value. This section will address the performance or expected performance of the GFIG in terms of an experimental evaluation of the system in the laboratory. Both electro-optic and acousto-optic methods of phase modulation were investigated.

8.1 Electro-Optic Phase Modulation

In Section 5.3., it was seen that electro-optic phase modulation limited the GFIG to a pointing accuracy of about 2°. The amplitude stability of the drive oscillator (0.002%) was determined to be the limiting factor in that section.

However, it should be remembered that the Pockels cell phase modulator is a birefringent element (uniaxial with no applied electric field and biaxial in the presence of an electric field). The birefringent element is a small, rectangular piece (3 mm x 4.5 mm x 26 mm) of ADP immersed in an index matching fluid and mounted in a cell containing two windows (the external faces of the windows were anti-reflection coated to reduce Fresnel reflections). The modulator was a transverse type in which the applied field was perpendicular to the direction of propagation in the crystal. The crystal was cut in what is known as a 45° x-cut (Figure 24).

$\vec{x}, \vec{E}_x$

$\vec{k}, \vec{z'}$ (direction of propagation)

45°

45°

$\vec{z}$

$\vec{y}$

$\vec{y'}$
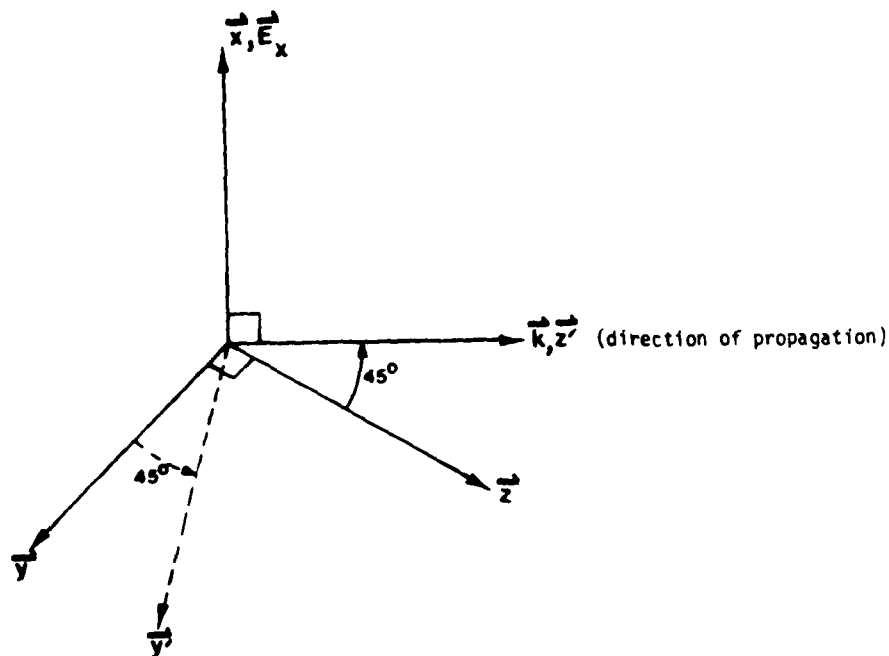
Figure 24.   Geometry of 45° x-cut ADP phase modulator crystal.

In Figure 24, $\vec{x}$, $\vec{y}$, and $\vec{z}$ are the orientation of the crystallographic axes in the absence of an applied field. $\vec{x}$ is parallel to the face of the crystal while $\vec{y}$ and $\vec{z}$ are 45° with respect to the crystal faces. In the presence of an applied electric field (along $\vec{x}$), the axes are rotated thru 45°, i.e., $\vec{y} \rightarrow \vec{y'}$, $\vec{z} \rightarrow \vec{z'}$.

Ideally, if the polarization vector of the incident linearly polarized wave (propagating along the $\vec{z}'$ direction) is along $\vec{y'}$, then only the $\vec{y'}$ component will be phase modulated (any residual component along $\vec{x}$ will not be modulated).

Since a rotation phase shift is sensed and measured in terms of the strength of the 1st harmonic at the modulation frequency, any modulation in the fringe intensity at this frequency that is not related to rotation represents an error term. The performance of the modulator therefore has to be determined

in terms of any residual intensity modulation that is present on the beam after it emerges from the modulator. Measurements of the intensity modulation that were introduced by the modulator were made and the results were not encouraging. The intensity modulation present on the beam emerging from the modulator varied considerably, from an equivalent pointing error of about 0.04 deg to 8 deg. In no case, could the error be held at a low value for any reasonable length of time (i.e., on the order of minutes or more). There are several possible explanations for this intensity modulation. A possible one is that the transmission of the modulator may be variable. After all, its configuration is that of an etalon with a total of six reflective surfaces. Since the optical path of the inner element, the ADP crystal, is made to vary with an applied field, the effective transmission of the device varies also. However, the reflectivity at the crystal-matching fluid interface should be quite low since the refractive index of the matching fluid was chosen to match, as nearly as possible, that of the crystal. Another possibility, and a likely one at that, is that neither the crystallographic axes, nor the induced axes, are perfectly orthogonal. Measurements in the laboratory seem to confirm this hypothesis, as the intensity modulation is present both with and without a polarization analyzer. Any slight misalignment of the input polarization vector with respect to the y' axis would result in the propagation of two "orthogonal" modes thru the crystal, one that is phase-modulated and one that isn't. A misalignment in the analyzer could result in an interference of these two modes even if the crystal were perfect. However, a modulation is present without an analyzer. If the two modes (resulting from a misalignment of the input polarization vector) are not orthogonal, they can be made to interfere even without an analyzer to recombine them. This does seem to be the case with the modulator that was used in the GFIG. Discussions with the manufacturer did not preclude the possibility that the axes

51

are not quite orthogonal (to within a few minutes of are).

Since the intensity modulation was not constant, some mechanism needs to be invoked to explain the large dirfts (0.04 deg to 8 deg). Three possibilities are: (1) thermal changes in the crystal birefringence, (2) stress-induced changes in the birefringence, or (3) the presence of fringing electric fields. Both (1) and (3) were investigated but no conclusions could be drawn since the drifts were so rapid that cause-and-effect relationships could be drawn since the drifts were so rapid that cause-and-effect relationships could not be established. Item (2) could not be investigated.

Aside from the "intrinsic" intensity modulation that the phase modulator produced, even more pronounced effects were observed when the beam was focused onto the fiber. A detector placed at the opposite fiber end registered an intensity modulation equivalent to 180 - 320° pointing accuracy. The explanation for this large error seems obvious, an angular dither of the beam that is large enough to change the coupling into the fiber. This effect could arise from: (1) improper alignment of the beam into the crystal, (2) lack of orthogonality between crystal axes, and (3) inaccurate cutting/preparation of the crystal. Improper alignment of the beam to the crystal did not seem to be the reason for the large intensity modulation since adequate alignment freedom and adjustment were available. Also, the final alignment was adjusted to provide minimum modulation. In view of the previous discussion re orthogonality of cyrstal axes and the now critical 45 deg x-cut for the two end faces of the crystal, it would seem that possible deficiencies in the manufacturing and fabrication of the electro-optic device itself are among the critical factors to the success of the phase modulation technique.

8.2 Acousto-Optic Phase Modulation

Although it was pointed out in Section 4.3 that the technique of acousto-optic phase modulation suffers a serious limitation in an all discrete system, the technique was nonetheless experimentally evaluated in the GFIG configuration. The reason for doing so was based on the fact that the electro-optic method of phase modulation limited the performance of the GFIG to about 180 - 320 degrees pointing accuracy. Any significant improvement in this performance would be a factor in its favor.

The frequency offset required for a $\pi/2$ phase bias was calculated to be 32.76 kHz for a 1.57 km long fiber. The angular dither that was associated with this amount of frequency modulation (f_c = 90 MHz) is equivalent to a pointing error of 12 - 550 degrees. Thus, in a discrete system, this method is no better than the electro-optic technique of phase modulation.

8.3 Overall Performance

The sensitivity of the GFIG (with phase modulation) to low rotation rate sensing was not determined. This was due to the fact that the system was not free of nonreciprocal phase biases unrelated to rotation (the nonreciprocal phase bias due to angular misalignment between the two output beams was much larger than the phase shift due to rotation).

However, the sensitivity of the system was evaluated by biasing the interferometer to $\pi/2$ with a rotation of approximately 1.8 deg/sec and determining the fringe resolution at that point (insofar as performance is concerned, this should be equivalent to biasing to the same level with an electro-optic or acousto-optic phase modulator). The measured resolution was about 0.004 fringe or equivalently 0.03 deg/sec for the 1 m diameter, 1.57 km long fiber coil, i.e., approximately 10 times earth rate.

53

The resolution of 10 Ω_E is about 2 - 5 times less than that expected. The discrepancy is likely due to drifts associated with coupling efficiency into the fiber, since discrete components were used, and due to source intensity changes.

9.0 DISCUSSION

The purpose of this section is to address the basic concept of the passive interferometer used as a rotation sensing device. The validity of the Sagnac effect is well established.[1-5] The application of the Sagnac effect to ring-laser rotation sensors having inertial grade characteristics is now a scientific fact as well as a commercially established endeavor. Only recently has a passive interferometer fiber-optic gyro sensed earth rotation (since this current work was completed). The enthusiasm over the fiber optic laser interferometer gyro is related to the potential for long life, low weight, small volume, low power, low cost, instant turn-on, no lock-up, integrated systems, etc.

The so-called "photon noise limited sensitivity" depends upon geometrical parameters, fiber attenuation, laser power, wavelengths, and the model used for the signal-to-noise calculations. The following section will discuss the photon noise limit as the criterion for sensitivity. Next, the passive interferometer gyro concept will be discussed. Finally, the question of discrete vs hybrid vs fully integrated fiber interferometer rotation sensors will be discussed.

54

9.1 Comment on the Photon Noise Limit as the Criterion for Ultimate Gyroscope Sensitivity

The term photon-noise limit is somewhat a misnomer. Shot noise limit (of the photodetector) is more appropriate since the signal-to-noise calculations are based upon it.

Impetus to the shot noise limit as the ultimate criterion for gyroscope performance had its origins in a 1971 paper by Moss, Miller and Forward[17] who described a photon-noise-limited gravitational antenna. Basically, their device was a Twyman-Green laser interferometer that was allegedly well-isolated from its thermal and mechanical environment. In that experiment, the optical path length of one interferometer arm was allowed to vary by subangstrom amounts by applying an AC voltage to a pizeoelectric driven mirror and recording the corresponding change in the fringe intensity that resulted when both beams were recombined. Although one may have reservations about such an experiment, let it be assumed that a cause-and-effect relationship was indeed observed (change in fringe intensity with a change in optical path length in one interferometer arm). It is therefore conceivable that a photon noise limited (i.e., shot noise) deflection was observed.

However, this is the point that some researchers may have overlooked. A fringe shift was not directly measured. The fringe shift was known beforehand (or calculated afterwards) from the transfer function of the pizeoelectric element. In order to <u>infer</u> a fringe shift from the measured change in fringe intensity, the <u>full dynamic range</u> of fringe intensity (from maximum to minimum) would have to be known to at least as many significant figures as the smallest resolvable change in intensity. Furthermore, since the fringe intensity is not a linear function of the fringe shift (a cosine function is involved), an accurate <u>measure of the induced fringe shift</u> would have to include a prior knowledge, i.e., measure (and an accurate one at that), of whereabouts on the intensity curve the incremental change had taken place. Since Moss, *et al.*, were not at that time concerned with a direct measure of the fringe shift, a simple solution to the problem of resolution in the cause and effect measurement presented itself (just bias the signal until the required resolution is achieved). This topic will be discussed in the following section.

The shot-noise limit as a measure of gyroscope performance can be questioned from another point of view (the preceding discussion has already indicated that resolution in a fringe intensity measurement is the deciding factor). In Appendix A, the shot-noise limited performance (i.e., fringe shift resolution) was determined to be:

$$\Delta Z)_{min} = \frac{\sqrt{B}}{\pi} \sqrt{\frac{2h\nu}{nP_o e^{-\alpha L}}} \, , \quad \phi_B = 0 \, , \tag{1}$$

$$\Delta Z)_{min} = \frac{\sqrt{B}}{\pi} \sqrt{\frac{h\nu}{nP_o e^{-\alpha L}}} \, , \quad \phi_B = \frac{\pi}{2} \, . \tag{2}$$

56

From these expressions, it is seen from the shot-noise limit point-of-view, that it matters little ($\sqrt{2}$ improvement) where or not the system is biased to the point of maximum sensitivity on the I vs. Ω curve (Figure 6). The explanation is as follows: Although a signal-to-noise ratio in general increases as the square root of the total power falling on the detector (P_o in the above expressions is the output of the laser, not the total power falling on the detector), the noise in the signal itself actually increases (as the square root of the signal power). With this increase in total noise, the resolution in a fringe intensity measurement (which depends on the difference between signal levels) departs from the usual expression. The net result is that the minimum resolvable fringe shift (based on shot-noise) is relatively independent of whether or not the system is biased.

Consider now the case where $P_o \rightarrow \infty$. In this case, $\Delta Z)_{min} \rightarrow 0$, whether or not there is a phase bias. However, it was seen earlier (Section 4.0) that it is advantageous to bias the interferometer to the point of maximum slope since this is where the sensitivity is greatest. There now exists what might be called a paradox: with an infinite signal-to-noise ratio, based on the shot-noise limit, it does not seem to matter whether or not the system is biased. However, from the point of view of resolution, it matters significantly.

At this point, the decision must be made whether or not to accept the shot-noise limit point of view as the ultimate criterion for gyroscope sensitivity. We contend, based on the above arguments, that the so-called "photon noise limit" does not represent the ultimate gyroscope sensitivity. Indeed, the ultimate sensitivity is intimately related to the resolution in fringe intensity that is available experimentally. With 16-bit resolution, the pointing error of the GFIG (Figure 1) is approximately 2 degrees and with 20 bits, it is only 5 min.

9.2 Comment on the Passive Interferometer Gyro Concept

Techniques requiring a measurement of the fringe intensity to back out a rotation rate have been shown to have limitations. Some of these limitations involved the components of the signal processing electronics and the devices for producing phase modulation.

The most serious limitation discussed so far is that related to the resolution requirement on the fringe intensity measurement. Some researchers[18] have claimed that sufficient resolution can be achieved by biasing the signal with a DC potential and increasing the gain of the electronics. However, the full dynamic range of the fringe intensity (from maximum to minimum) must be known to as many significant figures as is required for the desired resolution. Therefore, any bias voltage that is applied must be measurable to approximately the same degree of resolution. Also, the bias must be free from any drifts. Another suggestion for obtaining sufficient resolution is based on a series or parallel arrangement of analog-to-digital converters. Furthermore, the biasing technique may defeat any method used to handle source intensity fluctuations, a problem that is discussed below.

A difficulty with the passive interferometer gyro concept is the handling of source intensity fluctuations. A phase (or rate) measurement in many of the fiber-optic gyro devices is based on a change in fringe intensity. Any effect that gives rise to an intensity change is inditinguishable from a change due to rotation.

There are two sources of intensity fluctuations and drifts. These are: drifts in the laser output power and, in the case of discrete systems, coupling changes into the fiber due to thermal and mechanical instabilities. Drifts in the laser output power amount to about 1 - 2% for unregulated gaseous lasers. The figure for unregulated solid state lasers is about the same. It is possible that these drifts cou d be held to better than 0.1% in regulated systems. Coupling efficiency dirfts are about the same in descrete systems.

Some researchers have suggested that intensity fluctuations could be handled by either differencing the signals from two detectors monitoring complementary fringe patterns[9,14,15], or by ratioing the difference to the sum signal formed by the two detectors monitoring the same complementary fringe patterns (two beamsplitters are used instead of one in order to form the two interference patterns). Lin[9,14], has suggested that source intensity fluctuations are a form of common-mode noise and that rejection can be achieved by forming the difference signal.

One method proposed by Goss and Goldstien[6] is based upon the ratioing of the difference signal to the sum signal formed by detectors looking at two complementary fringe patterns. The two signals may be represented by:

$$S_1 = A \, P_o (1 - m \, \sin\phi_r) + S_o \, ,$$

and   (3)

$$S_2 = A' \, P_o (1 + m' \, \sin\phi_r) + S_o' \, .$$

59

In the previous expression, P_o is the fluctuating laser power and A, A are collective terms containing parameters related to: detector responsivity, amplifier gain, beamsplitter transmissions and reflectivities, fiber and modulator transmissions, and coupling efficiencies. S and S_o' are offsets due to detector dark current and amplifier offset. m and m' are the visibilities of the fringe pattern and are determined by the beamsplitting ratio and coupling efficiencies. The visibilities are not in general equal to 100% and likewise they are not necessarily equal to one another.

In order to form a meaningful ratio, the offsets S_o and S_o' must first be set to zero. This requirement is difficult in a DC detection system and is due to the fact that offsets in a DC system are difficult to control. Although the Goss-Goldstein system utilizes phase sensitive (synchronous) detection, demodulation does not occur until after the sum and difference signals are formed (if demodulation were to occur prior to ratioing, it is still difficult to have two synchronous detectors with the same characteristics). Their technique requires that each of the two signals (biased to $\pi/2$ as evidenced by the sin term in Equation (3)) be digitized prior to formation of the ratio. Thus, the two fluctuating signals must both be resolved with high resolution to achieve the desired rate (phase) sensitivity. The resolution requirements have been enumerated elsewhere and not repeated here.

Another method that has been proposed to eliminate source/coupling drifts and fluctuations is based on analog ratioing devices. These devices presently are noisy and the amount of noise that they introduce exceeds the shot-noise of the detectors by several orders of magnitude.

In summary, the passive interferometer gryoscope concept is seen to suffer from a number of difficulties. The most fundamental is the resolution in fringe intensity required of these devices. Additionally, the engineering problem cf source intensity fluctuations limits its sensitivity. One possible means by which the performance and sensitivity of a fiber-optic rotation sensing device can be improved is suggested in the next sections.

9.3 Discrete vs. Hybrid or Fully Integrated Fiber-Optic Interferometer Rotation Sensors

A number of advantages have been attributed to the fiber-optic interferometer gyroscope, especially in the form of an all integrated system (Section 9.0). To recapitulate, some of the advantanges are: long life, low weight, small volume lower power, low cost, etc. However, it should be pointed out that these advantages are meaningless unless the device is capable of meeting the drift requirements for the particular application for which it has been designed.

The meeting of a drift requirement is not, however, determined solely by the fact that the gyroscope may be integrated. The ability to discriminate small phase shifts (and to achieve low drift rates) in terms of intensity changes depends mainly upon the resolution in the measurement of fringe intensity and upon source fluctuations. Four major advantages to an integrated system are: (1) Stabilization of the input power that is coupled into the fiber as mechanical fiber holders, lens mounts, and other such devices tend to move about somewhat. (2) No need to align the two output beams to subnanoradian accuracy as both outputs are mutually coupled. Therefore, there is no drifting non-reciprocal phase shift. (3) Acousto-optic phase (frequency) modulation may

61

be used (in higher rate applications) since beam deflection and its resultant effect on power coupling may be significantly reduced. (4) Furthermore, there is no need for constant realignment.

One thing that an integrated optics system will not do is overcome the shortcomings of an electro-optic phase modulator. The effects of beam motion will be reduced (possibly eliminated), although it is doubtful that a modulator free from the problems discussed in Section 8.1 could be manufactured in integrated form.

Thus, while an integrated or hybrid (discrete only from fiber to detector) fiber-optic rotation sensor offers some potential improvement over a discrete system, it has to be pointed out that the key to a successful device lies in signal processing and not packaging, etc. One such system in which shot-noise limited performance might possibly be obtained is discussed in the following section.

9.4 Suggestions for Improvement

It was seen in Section 8.0 that the techniques for introducing phase modulation suffered from limitations of one sort or another. Furthermore, most of the techniques discussed in Section 4.1 for phase biasing a fiber interferometer had one problem or another. Additionally, the author of this report believes the method for handling source intensity fluctuations (Section 9.2) are not sufficient.

Thus, a method based upon the extraction of rate information from a relative measure of fringe intensity does not appear to have any merit in low rate applications requiring inertial grade quality.*

There is at least one method left in which shot-noise limited performance many be approached in a fiber-optic interferometer gyroscope. This method

---

*Note added in proff: This is not necessarily true for other applications such as guidance and control functions.

is based on the nonreciprocal approach utilizing acoustic-optic frequency shifters and was discussed in Section 4.1. Frequency stability requirements for these devices were discussed in Section 5.3. Instead of using this technique for introducing a nonreciprocal phase bias which biases the intensity of the fringe to the point of maximum slope on the I vs. Ω curve (Figure 6), the bias phase introduced by the A/O frequency (phase) shifters is used to cancel the nonreciprocal phase shift due to rotation (and any other sources of nonreciprocal phase shift) thus moving the nominal operating point to the point having zero slope. If the system drift is determined primarily by the shot-noise limit (and not by resolution in the fringe intensity measurement), then it matters little whether the system is nulled to the point of zero slope or maximum slope (at $\pi/2$). This consideration was discussed in Section 9.1. However, by moving the operating point to the null, the effect of source intensity fluctuations are greatly reduced. Additionally, the requirement on fringe intensity resolution drops out of the picture since the full range of fringe intensity (from minimum to maximum) is not required to back out the resultant phase. Thus, the system gain can be arbitrarily increased as required in order to detect the cause-and-effect relationship due to phase nulling.

Rate information is obtained by equating the fringe shift required to produce a null, i.e.

$$\Delta Z = \frac{nL}{c} \Delta f \quad , \tag{4}$$

to the fringe shift due to rotation:

$$\Delta Z = \frac{2LR}{\lambda c} \Omega \quad . \tag{5}$$

63

Equating,

$$\Delta f = \frac{2R}{\lambda n} \Omega \quad . \qquad (6)$$

Equation (6) shows that the frequency shift Δf needed to compensate for a rotation rate does not depend on the length of the fiber coil. This fact is an important one since short fiber lengths may be used, thereby increasing the S/N ratio since more power can be delivered to the detector. This aspect is, of course, in direct contradiction to that concluded in References 7, 8, 9, 14. In those treatments, it was inferred that an optimal fiber length existed. The analyses were based on the assumption that the rotational phase shift could only be deduced from a fringe intensity measurement. This, of course, is not required in the phase nulling technique.

At this point it should be emphasized that the phase nulling technique outlined above is not an original one and is based on the method suggested by Davis and Ezekiel[11] and Cahill and Udd[13].

Figure 25 is a tentative schematic outline of a fiber-optic interferometer rotation sensor based on the above considerations.
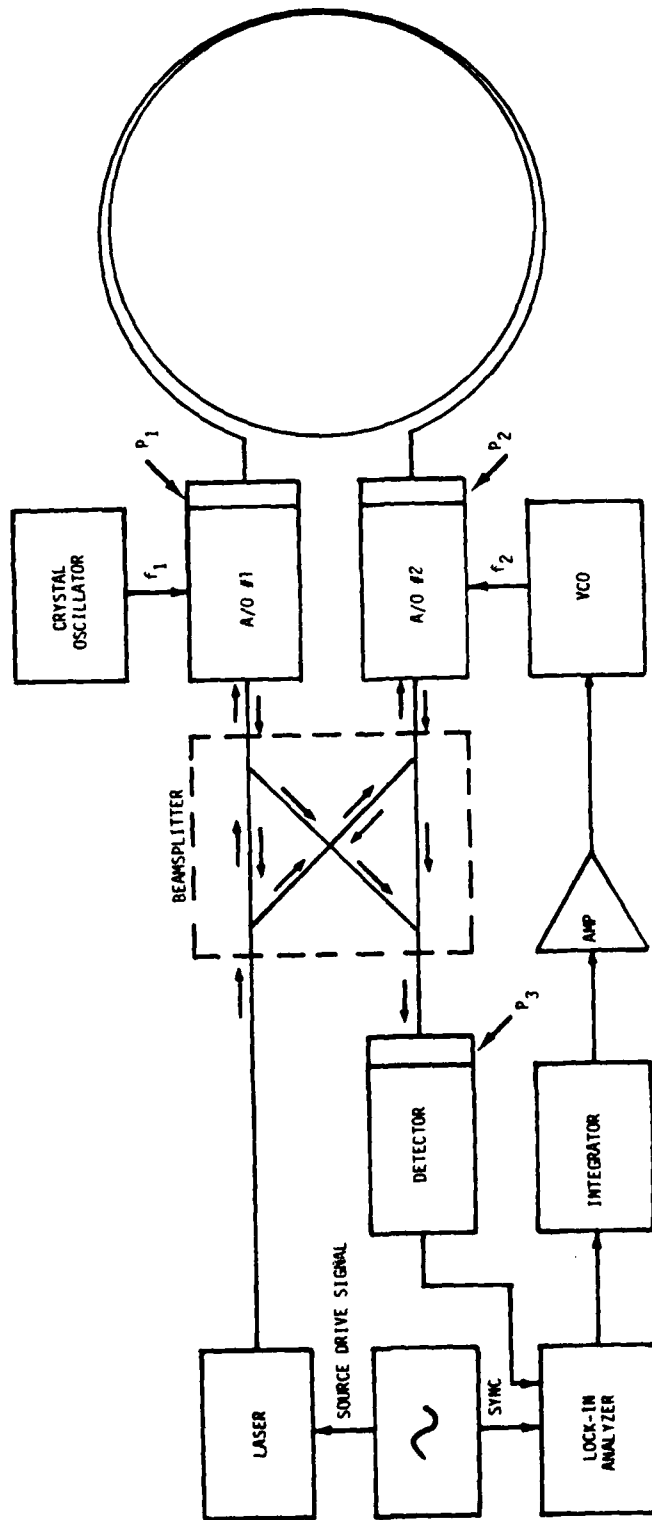
Figure 25. Improved fiber-optic rotation sensor (conceptual).

The system that is envisuaged is a partially integrated one (hybrid) or an all integrated system. The key point, whether hybrid or integrated, is that discrete optical/mechanical components are avoided. Even a hybrid system should avoid the usage of opto-mechanical devices (positioners, etc.) to couple optical power from one device to another; at least, permanently affixed short pieces of fiber should be used.

The beamsplitter in Figure 25 is a waveguide device. Also, acousto-optic frequency shifters #1 and #2 are of an integrated variety on a single chip. The purpose of polarizers #1 and #2 is to insure that only one mode of propagation is allowed in the fiber (if two polarization modes were involved, a nonreciprocal phase shift between the two propagation directions could result since the fiber is birefringent). Polarizer #3 is required in order to guarantee a high fringe visibility.

The success of the above suggested technique depends on several factors. Of primary importance is the beamsplitter - it must be capable of providing an exact equal split of energy into the two fiber ends as well as an equal split upon their return. In other words, the fringe visibility must be as near to 100% as possible (any deviation from 100% will reduce the sensitivity on the device as well as reflect source intensity fluctuations).

Stability requirements on the driver for the acousto-optic phase shifters have been given elsewhere (Section 5.3).

1/f type noise and the effect of amplifier offsets can be reduced by chopping the source (in Figure 25, intensity modulation via an alternating source voltage is utilized) and synchronously detecting the intensity of the fringe pattern.

Summarzing, the above method utilizing phase nulling techniques (without phase modulation) appears to be at least one capable of producing shot-noise

66

limited performance.

10.0 SUMMARY

This report describes a development effort aimed at perfecting a North-seeking device based on the passive interferometer gyroscope (discrete) concept.

A number of concepts by which the sensitivity of a fiber-optic interferometer could be improved are review and the limitations of the various techniques are addressed. Specifically, phase modulation techniques utilizing electro-optic and acousto-optic devices are discussed. The limitations of these devices were experimentally determined. In particular, it was found that the intrinsic intensity modulation produced by these elements in a discrete system precluded their usefulness in any system requiring <u>inertial</u> grade performance but not necessarily for certain guidance and control systems.

The basic concept of a fiber interferometer as a rotation sensing device is also addressed. The concept has certain limitations if rate information is to be extracted in the form of a fringe intensity measurement. The limiting factors are the resolution requirement on the fringe intensity measurement and the methods utilized to compensate for source intensity fluctuations.

Finally, the performance of a fiber-optic interferometer is discussed in term of the photon-noise limit. This is the limit to performance that several researchers have used in arriving at the performance of a passive interferometer laser gyroscope. This concept has a number of restrictions. First and foremost are the resolution requirements on the fringe intensity measurement (if rate information is to be extracted from an intensity measurement). Secondly, the methods for compensating for source intensity fluctuations are found to constrain

67

the sensitivity to a value above that predicted by the photon noise limit.

Section 9.4 concludes with a suggestion by the author of this report, for a method in which the photon noise limit might be approached.

11.0 REFERENCES

1. G. Sagnac, Comp. Rend. 157, 708, 1410 (1913).

2. See, for example, P. Harzer, Astronom. Nachrichten 198; B. Pogany, Annalen d. Physik 85, 244 (1928); H. Thirring, "Handbuch der Physik", 12, 344, Springer, Berlin 1927, A. Sommerfeld, "Optik", 3rd ed., Akad. Verlagsges., Leipzig, 1964.

3. E. J. Post, Rev. Mod. Phys. 39, 475 (1967).

4. A. A. Michelson and G. Gale, Nature 115, 566 (1925); Astrophys. J. 61, 137 (1925).

5. V. Vali and R. W. Shorthill, Appl. Optics 15, 1099 (1976).

6. W. C. Goss and R. Goldstein, Optical Engineering 18, 9 (1979).

7. V. Vali and R. W. Shorthill, SPIE Proceedings 77, 110 (1976).

8. R. Goldstein and W. C. Goss, Jet Propulsion Laboratory, Internal Memorandum (1977).

9. S. C. Lin, Appl. Optics 18, 915 (1979).

10. R. Goldstein and W. C. Goss, Optical Engineering 18, 381 (1979).

11. J. L. Davies and S. Ezekiel, SPIE Proceedings 157, 131 (1978).

12. J. L. Skripka and R. J. Fredricks, Final Technical Report, Contract N00014-74-C-0382, Office of Naval Research, Washington, D. C., April, 1975.

13. R. F. Cahill and E. Udd, Optics Letters 4, 93 (1979).

14. S. C. Lin, SPIE Proceedings 157, 149 (1978).

15. M. N. McLandrich and H. E. Rast, SPIE Proceedings 157, 127 (1978).

16. V. Vali and M. F. Berg, SPIE Proceedings 157, 120 (1978).

17. G. E. Moss, L. R. Miller, and R. L. Forward, Applied Optics 10, 2495 (1971).

18. W. C. Goss, Jet Propulsion Laboratory, California Institute of Technology, private communication.

APPENDIX

A. Derivation of the Shot-Noise Limited Fringe Detectibility

The minimum detectable fringe shift, assuming adequate instrument resolu-
tion, is determined by the shot noise that is always present in a measurement
of this type. The ability to discriminate a small phase change depends upon
the ability to discriminate the resultant change produced in the fringe intensity.
Consider the situation depicted in Figure 26.
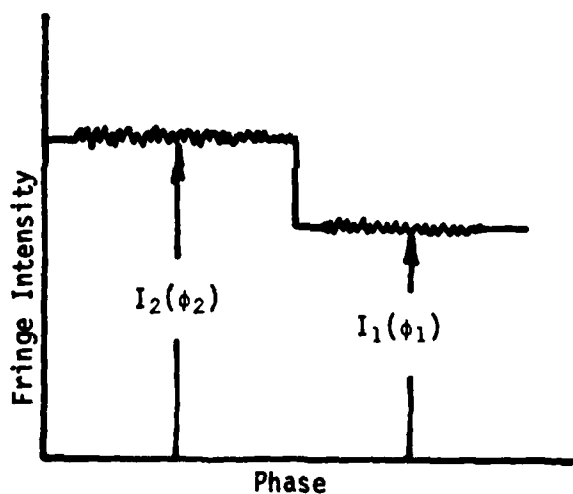
Figure 26. Intensity vs. Phase.

Since the signal of interest is the small differential change in fringe
intensity, the signal may be written as

$$\Delta I = I_2 - I_1 \qquad (1)$$

If I represents the photodetector current, then

$$\Delta I = \frac{\eta e}{h \nu} (P_2' - P_1') \quad , \tag{2}$$

where P_1' and P_2' are the optical powers falling on the detector. h, e, and ν are Plank's constant, the electronic charge, and the frequency of the optical wave respectively. η is the overall efficiency and may be written as

$$\eta = \eta_p \, \eta_R \, \eta_c \quad . \tag{3}$$

η_p is the quantum efficiency of the detector, η_R = reflection efficiency of the beamsplitter, and η_c is the coupling efficiency into the fiber.

The optical power, P', in the fringe pattern falling on the detector may be written as

$$P' = \frac{P_o \, e^{-\alpha L}}{2} (1 - \cos\phi) \quad . \tag{4}$$

In (4), P_o is the output of the laser, α the attenuation of the fiber, and L the fiber length. ϕ is the phase between the two recombined beams. Combining Equations (2) and (4), the signal may be written as

$$S = \frac{P_o \, e^{-\alpha L} \eta e}{2 h \nu} (\cos\phi_1 - \cos\phi_2) \quad . \tag{5}$$

If there is a bias phase, ϕ_B, (5) becomes

$$S = \frac{P_o \, e^{-\alpha L} \eta e}{2 h \nu} [\cos\phi_B - \cos(\phi_B + \Delta\phi)]. \tag{6}$$

where $\phi_1 = \phi_B$ and $\phi_2 = \phi_B + \Delta\phi$. $\Delta\phi$ is the phase shift that is to be resolved from the fringe intensity measurement.

The shot noise current, N, associated with the photodetection process is

$$N = \sqrt{2eI_2B} \quad , \tag{7}$$

where B is the system bandwidth. I_2 has been used since it represents the signal current associated with the small phase shift, $\Delta\phi$, that is being measured. Now,

$$I_2 = \frac{P_o e^{-\alpha L} \eta e}{h\nu} [1 - \cos(\phi_B + \Delta\phi)] \tag{8}$$

Thus, the noise current may be written as

$$N = \sqrt{\frac{\eta e^2 B P_o e^{-\alpha L}}{h\nu} [1 - \cos(\phi_B + \Delta\phi)]} \tag{9}$$

Combining Equations (6) and (9), the signal-to-noise ratio may be expressed as

$$S/N = \sqrt{\frac{\eta P_o e^{-\alpha L}}{4h\nu B[1 - \cos(\phi_B + \Delta\phi)]}} \; [\cos\phi_B - \cos(\phi_B + \Delta\phi)] \tag{10}$$

The minimum detectible fringe shift may be determined by setting S/N = 1. Recalling that

$$\Delta Z)_{min} = \frac{\Delta\phi)_{min}}{2\pi} \quad , \tag{11}$$

the minimum fringe shift is found to be

$$\Delta Z)_{min} = \frac{\sqrt{B}}{\pi} \sqrt{\frac{2h\nu}{\eta P_o e^{-\alpha L}}} \quad , \quad \phi_B = 0$$

$$\Delta Z)_{min} = \frac{\sqrt{B}}{\pi} \sqrt{\frac{h\nu}{\eta P_o e^{-\alpha L}}} \quad , \quad \phi_B = \frac{\pi}{2} \qquad\qquad (12)$$

$$\Delta Z)_{min} = \frac{\sqrt{B}}{\pi} \sqrt{\frac{8h\nu}{\eta P_o e^{-\alpha L}}} \quad , \quad \phi_B = \pi$$

From the above expressions, it is seen that little is to be gained by biasing the fringe intensity to the point of maximum slope if shot noise is the only limiting factor.